Renewable and Sustainable Energy Reviews 173 (2023) 113102

Contents lists available at ScienceDirect

Renewable and Sustainable Energy Reviews

journal homepage: www.elsevier.com/locate/rser

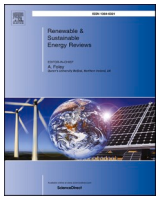

Formate/bicarbonate interconversion for safe hydrogen storage: A review

M. Calabrese, D. Russo *, A. di Benedetto, R. Marotta, R. Andreozzi

Dipartimento di Ingegneria Chimica, dei Materiali e della Produzione Industriale, Università di Napoli Federico II, P.le V. Tecchio 80, 80125, Naples, Italy

ARTICLE INFO

Keywords:
Hydrogen storage
Formate
Safety
Hydrogen
Bicarbonate
Kinetics

ABSTRACT

Formates are promising salts for hydrogen storage. They can be catalytically converted to bicarbonate at near-ambient conditions, and regenerated under moderate pressure for H_2 uptake. Moreover, the system is completely safe, non-toxic, and easy to handle. Up to date, a few heterogeneous catalytic systems have been proposed to carry this transformation. However, many criticisms still have to be addressed, including reaction kinetics for high power applications, stability, cyclability, and supersaturated solutions to increase energetic density. In this work, a critical review of the state of art of such system is presented, highlighting theoretical limitations and applicative shortcomings, and giving perspective on critical issues to be addressed in future research. Despite the actual bottlenecks, the system is still scarcely explored and there is promising room for improvement. State-of-the-art catalytic systems could provide 72% energetic efficiency, that could be improved up to 90%.

1. Introduction

Hydrogen is widely recognized as a valuable resource for the development of environmentally friendly energy generation technologies [1–3]. Combustion of hydrogen only generates water, reducing greenhouse effects due to emissions by motors and gas turbines [4]. In this sense, a complete product life cycle analysis should be performed [5,6], including any emission from the hydrogen production process, which is currently primarily obtained from methane reforming [7]. This difficulty can be solved by directly or indirectly producing hydrogen from nuclear energy or renewable sources [8–10]. This would solve the CO_2 emission problem at the source.

According to Mission Innovation, the hydrogen sector is one of the most important areas for achieving decarbonisation by 2050 [11]. In this regard, the European Commission has launched the European Clean Hydrogen Alliance [12], a public-private partnership that brings together industry leaders, civil society, national and regional ministers, and the European Investment Bank to identify hydrogen technology needs, investment opportunities, and enablers.

In addition to the previously mentioned advantages of hydrogen production as a green energy source, the growing interest is fueled by a number of other positive and beneficial factors, including: a higher energy density per unit mass than batteries, allowing it to be used for long-distance transportation and heavy goods [13,14]; long-term storage; transportation options that make use of existing infrastructure [14–17]; and distribution with low adaption costs [4].

However, some problems still remain that hinder the development of a hydrogen economy. One of these is represented by storage [18–20], which traditionally necessitates high pressures and/or cryogenic temperatures [21–24].

As a result, it is believed that one of the most difficult tasks to favor the hydrogen economy future expansion is the discovery of safe and efficient hydrogen storage systems. Innovative approaches that propose the use of materials capable of ab/ad-sorbing or chemically binding hydrogen in a reversible way, restricting the operating pressure to lower values than traditional compressed storage are gaining attention in the scientific community [25–29]. The rising interest of the scientific community in this topic is shown by the large number of review papers dealing with hydrogen storage techniques published in the last ten years for both mobile and stationary applications [30–43]. As an alternative to traditional cryogenic and/or pressure storage, hydrogen can be stored by physical adsorption, in porous and solid materials such as graphene and other carbon structures, composites like metal-organic frameworks (MOFs), and zeolites [36,44–46]. In particular, MOFs can store and release H_2 by working at 100 bar and 77 K, up to energetic densities of 7.2 MJL^{-1}. However, MOFs frequently become unstable after several cycles, they are air sensitive, and they suffer from inevitable structural defects [47,48]. On the other hand, chemical storage takes advantage of hydrogenation and dehydrogenation reactions to store and release hydrogen. Materials including light metal hydrides, liquid organi carriers (LOCs), metal borohydrides [24,49], metal alanates [50,51],

* Corresponding author.
E-mail address: danilo.russo3@unina.it (D. Russo).

https://doi.org/10.1016/j.rser.2022.113102
Received 18 July 2022; Received in revised form 18 November 2022; Accepted 30 November 2022
Available online 16 December 2022

Abbreviations

FA	Formic acid
PF	Potassium formate
SF	Sodium formate
AF	Ammonium formate
PB	Potassium bicarbonate
SB	Sodium bicarbonate
AB	Ammonium bicarbonate
TON	turnover number
TOF	turnover frequency
LOCs	liquid organic carriers
MOFs	metal organic frameworks
PD/AC	Pd supported on active carbon
Pd/r-GO	reduced graphene oxide as a support
Pd/PDA-rGO	Pd catalyst supported on a phenylenediamine-alkalized reduced graphene oxide
Pd–Au/PDA-rGO	bimetallic catalyst supported on a phenylenediamine-alkalized reduced graphene oxide
Pd/N,P–C	Double-doped carbon-based catalysts
Pd/NC	novel palladium nanoparticle catalyst based on mesoporous carbon doped with nitrogen
PdAl/PDNPore	nanoporous catalyst consisting of nanoporous bare Pd with a variable percentage of bare Al
Pd/mpg-C3N4	Pd nanocatalyst supported on mesoporous graphitic carbon nitride
PANI	novel polyaniline mesoporous-carbon-supported Pd nanoparticles
Pd/PDMC	mesoporous carbon products
kv-PdO/TiNTs	PdO nanoparticles with Kirkendall nanovoids uniformly supported on titanate nanotubes
Ag/Pd/TiOx/TiO2	Pd/Ag alloy that was modified with a TiOx shell supported on TiO2
Pd–Au/AC	Pd–Au alloy nanoparticle supported on activated carbon

ammonia borane [52], metal amides [52], and amine metal borohydrides [53,54] are examples of materials with a high theoretical density [55–58]. Simple magnesium hydrides, transition metals, and complex metal hydrides - which often comprise Na, Li, Ca, Al, or B - are hydrides that have been suggested for use in the hydrogen economy. The materials with the best promise for solid-state hydrogen storage are metal hydrides like MgH_2 and $NaBH_4$. The latter has also been recently proposed for a novel coupled hydrogen-storage-and-production process [59–63]. However, hydrides have drawbacks, including the need for complex thermal management during hydrogenations and dehydrogenations, the need to work at low H_2 pressures during hydrogenations, frequently insufficient kinetics for high-power applications. LOCs have a lower practical barrier than other storage media, since they can take advantage of well-established infrastructure for storage, trasportation, and handling of gasoline and organic solvents. They have high energy densities of up to 7.7 MJL^{-1}, but require catalysts and usually are flammable and toxic.

Given the high storage capacity, gentle dehydrogenation conditions, and good stability at room temperature, aqueous solution of formic acid (HCOOH, FA) [64] and formic acid salts (formates) [65–69] are of interest for H_2 storage. Specifically, these systems offer great advantages from a safety point of view, overcoming the limitations of most storage systems mentioned above. In fact, traditional high pressure and/or cryogenic liquid hydrogen can generate a large number of accidental scenarios from cold clouds to physical explosions, flash fire, jet fire, fireball, and vapor cloud explosions [70]. On the other hand, less mature technologies like the above-mentioned MOFs, hydrides, LOCs, and other chemicals can generate accidents from difficult thermal management, react explosively with air humidity, be toxic, flammable, corrosive, and/or generate exothermal runaway reactions [22,30].

This review will focus specifically on formate aqueous solutions. Considering the emerging growing interest in this area, there is still a gap in the literature summarizing all the relevant catalysts, their preparation, their performances, and potentialities with respect to its technological application that may guide future research on the system. Due to its relatively high hydrogen storage volume density at ambient pressure (53 $gH_2\ L^{-1}$), formic acid was used in the first studies [71]. However, although FA dehydrogenation is the main reaction pathway (eq. (1)) for hydrogen generation, it also produces carbon dioxide, which is an unwanted side product. In addition, formic acid can undergo the dehydration reaction (eq. (2)), which produces H_2O and CO, the latter of which is poisonous to the adopted catalysts. Both dehydrogenation and dehydration of liquid FA are endothermic and exergonic, under normal reaction conditions.

$$HCOOH \rightarrow H_2 + CO_2 \Delta G^\circ = -0.34eV \Delta H^\circ = +0.30eV \quad (1)$$

$$HCOOH \rightarrow H_2O + CO \Delta G^\circ = -0.13eV \Delta H^\circ = +0.32eV \quad (2)$$

Because the variations in free energy and Gibbs enthalpy are so minor between the two processes [65], selective dehydrogenation of FA to H_2 requires careful manipulation of the reaction conditions and/or the use of suitable catalysts. Instead of FA salts, formates can be used to overcome these two issues (eq. (3)).

$$HCOOM + H_2O \leftrightarrow H_2 + HCO_3M \quad (where\ M = alkali\ metal) \quad (3)$$

Hydrogen release by formate dehydrogenation is a reversible method of hydrogen storage that does not emit CO_2, 3. Fig. 1. There are no unwanted side-reactions, and since the free energy change of the cyclic formate-bicarbonate conversion is nearly zero at near-ambient conditions, the equilibrium can be shifted by small reaction conditions changes.

One downside of formates is that they have a lower volumetric density than FA, but they are non-corrosive, non-irritating, and easier to handle. The primary FA salts have volumetric H_2 densities of 16.8 $gH_2\ L^{-1}$ for sodium formate (HCOONa, SF), 29.0 $gH_2\ L^{-1}$ for potassium formate (HCOOK, PF), and 21.2 $gH_2\ L^{-1}$ for ammonium formate ($HCOONH_4$, AF) [72].

This review will look at the thermodynamics and kinetics of the cyclic formate/bicarbonate system for hydrogen production. A summary of the thermodynamic analysis of the process will be followed by an assessment of the various types of catalysts that will define the kinetics

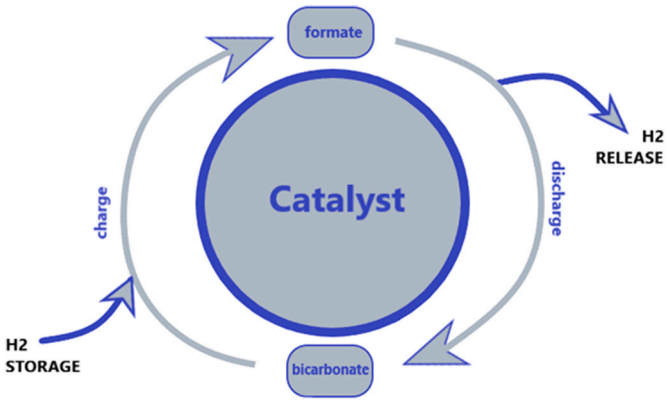

Fig. 1. Discharge and uptake reactions of the formate-bicarbonate cycle [42].

of the process, allowing for the determination of the most influential variables and the future needed investigation. Kinetic results reported in the literature are summarized and manipulated to assess the applicability of such a system for different technologies. Because of its applicative aim, in this review, homogeneous catalytic systems are not discussed, since they are not suitable for safe aqueous storage; they need solvents and expensive binders and offer limited recyclability and difficulty in recovery.

The review is structured as follow: in Section 2, the thermodynamics of the system and its limitations is summarized; in Section 3, an in-depth comparison of heterogeneous catalysts investigated in the literature is provided, summarizing performances, operating conditions influence, and achieved kinetics and comparing them on the base of applicative criteria.

2. Thermodynamics

Thermodynamics of the transformation define the limitations of such systems under different conditions. In fact, this system is particularly suitable for a cyclic transformation at near-ambient temperature because of the thermodynamic values of the equilibrium constants in the range 20–80 °C [73]. Thermodynamic analysis is a required step for evaluating and comparing the catalyst performances. Thermodynamic properties of the main salts are summarized in Table 1.

In particular, the temperature at which $\Delta G^0 = 0$ (eq. (3)) is 46 °C, 47 °C, and 52 °C, for sodium, potassium, and ammonium salts, respectively [74]. Forward dehydrogenation steps (eq. (4)) are slightly endothermic 19.4–49.4 kJ/mol and are thermodynamically favored at temperature higher than ~50 °C [74], where reaction kinetics are also faster.

$$HCOOM + H_2O \rightarrow MHCO_3 + H_2 \quad where\ M = Na, K, NH_4 \tag{4}$$

On the other hand, bicarbonate hydrogenation (eq. (5)) is favored at low temperature, and catalysts need to be optimized to work at the lowest possible temperature with considerable reaction kinetics. This is usually compensated by relatively high hydrogen pressure in the range 10–100 bar.

$$MHCO_3 + H_2 \rightarrow HCOOM + H_2O \quad where\ M = Na, K, NH_4 \tag{5}$$

A recently published thermodynamic analysis [74] highlights the role of different operating conditions and configurations on the maximum achievable conversion. The analysis was carried out in the range of concentration 0.1–5.0 mol L^{-1}, which is the common range adopted in the literature. The effect of the countercation on equilibrium calculations is not significant from a thermodynamic point of view. The results can be summarized as follows.

For a closed system, formate conversion to bicarbonates is hindered by high concentrations of salts, since the high concentration of released hydrogen pressurizes the headspace shifting the equilibrium towards the reactants. However, the absolute amount of released hydrogen, as well as its molar fraction in the headspace, increases with the initial concentration. The highest conversion (79.8%) in the range of temperature 20–95 °C in a closed system (with a headspace volume treble the liquid phase) is observed at 95 °C and 0.1 mol L^{-1} formate. For a 5.0 mol L^{-1} system under the same conditions, it strongly decreases to about 19.8%. However, the correspondent H_2 molar fractions in the headspace are 44.6% and 91.4%, respectively. Residual unconverted formate can hinder the cyclic transformation. However, a closed system is not the best applicative configuration, and it is mainly a reference for laboratory-scale catalytic tests. In any of the above cases, larger headspace volume favor conversion, but they can represent a serious drawback for applicative systems, since they reduce the overall volumetric energy density of the system.

For real application, a continuous system at a constant hydrogen pressure is the most desirable situation; in this case, at the highest investigated temperature and 5.0 mol L^{-1}, the maximum formate conversion decreases from 73.5% to 46.1%, when pressure is increased from 1 to 3 bars. In all practical situations, regular purge with inert gases can allow to achieve 100% thermodynamic conversion, but with hydrogen losses and/or reduced purity. A scheme of the reactor configuration is reported in Fig. 2. As mentioned in the study [48], most experiments in the literature are carried out in open or semi-open systems and results cannot be directly compared with thermodynamic calculations.

On the contrary, bicarbonate hydrogenation experiments are usually carried out in closed system charged with an initial H_2 pressure or keeping hydrogen pressure on the liquid phase constant, and a direct comparison is possible. Fig. 3 shows the best results reported in the literature using different catalysts, together with the thermodynamic limit under the adopted conditions. A full discussion of the reported catalytic systems is presented in Section 3, together with a full explanation of the adopted acronyms. From this comparison it can be seen that Pd supported on active carbon (Pd/AC) [46], on reduced graphene oxide (Pd/r-GO) [53], and on N/P doped carbon (Pd/N,P–C) [61] offer the best compromise in terms of performances and maximum achievable conversion. This cannot exclude that the other catalytic systems proposed in the literature might outperform the former if used under different operating conditions.

As a general trend, for hydrogenation reactions, thermodynamic calculations show that bicarbonate conversion, at 80 °C, increases with H2 pressure increasing from 56.9% to 72.5%, 81.5%, and 97.8% at 3.0, 6.0, 10.0, and 100.0 atm, respectively. The correspondent values at 20 °C are 85.5%, 92.2%, 95.1%, and 99.5%, and are all significantly higher. However, at this temperature reaction kinetics are usually much slower. Although conversion decreases with temperature, the effect is less marked at high pressure. Contrary to dehydrogenation, in this case, the initial concentration of bicarbonate does not significantly affect conversion values.

The thermodynamic analysis shows that at 5.0 mol L^{-1}, the maximum achievable energetic density is of about 9.5 KgH_2 m^{-3} corresponding to 1.4 MJ L^{-1}, about one half of the volumetric density of compressed hydrogen at 700 bar, but with undoubtedly increased safety. Moreover, this value could be reduced by the necessity of keeping the aqueous solution homogeneous, but it could be increased when dealing with heterogeneous solutions or when selecting salts like potassium or ammonium formate/bicarbonate, with a significantly higher solubility. A detailed discussion of solubility influence on energetic density is given

Table 1
-Gibbs free energy and enthalpy of formation of all primary salts of formic acid..

Species	$\Delta G^0_{f,298K}$ $\left(kJ\ mol^{-1}\right)$	$\Delta H^0_{f,298K}$ $\left(kJ\ mol^{-1}\right)$
$HCOONa\ (aq)$	−613.00	−666.67
$HCOOK\ (aq)$	−634.30	−677.93
$HCOONH_4\ (aq)$	−430.50	−588.06

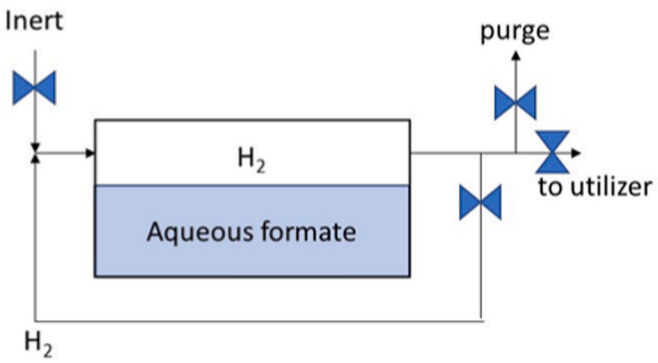

Fig. 2. Process scheme for semi-continuous pure hydrogen supply at constant pressure.

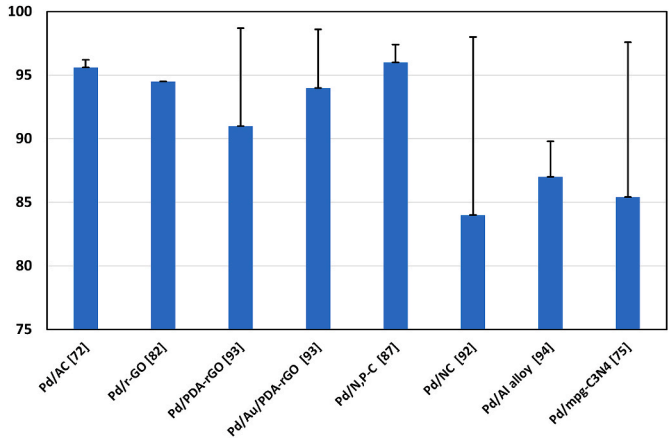

Fig. 3. Best performing catalysts reported in the literature (blue bars) compared to the theoretical maximum equilibrium conversion (red lines).

in Section 3.6. At present, there are no studies in the literature dealing with supersaturated solutions.

3. Performances of the catalysts proposed in the literature

Thermodynamics define limitations of the proposed system under certain conditions. The thermodynamic analysis suggests that once the optimal operating conditions are identified, the process can be performed with high conversions.

However, at present, the application of the proposed technology is practically limited by the lack of a catalytic system that is proven to be stable, cyclable, and that can perform the transformation with kinetics compatible with the requested power.

In general, both homogeneous and heterogeneous catalysts can be used, and each has its own set of benefits and drawbacks: homogeneous catalysts are more active, selective, and repeatable, but they are more difficult to recover, may require non-aqueous solvents, cost more on average, and are less resistant to thermal stress. Heterogeneous catalysts, on the other hand, are more temperature stable, simpler to recover, recycle, and regenerate, but they are less repeatable and active; however, they can be easily handled and all of them can be used in aqueous solutions. In this Section, a comprehensive review of the heterogeneous catalytic systems investigated for such transformation in aqueous solutions is provided [68,69,75–85].

The goal is to provide the state of the art in order to drive the design of catalysts that can optimize both reactions, resulting in a single cyclic system that can both uptake and release hydrogen.

3.1. Dehydrogenation reaction

Dehydrogenation of formates is:

$$HCOOM + H_2O \rightarrow MHCO_3 + H_2 \text{ where } M = Na, K, NH_4 \quad (4)$$

Transition metals, in particular palladium, are reported to be active phases capable of promoting this reaction. Palladium has demonstrated promising performances on a variety of substrates and when linked with other metals.

3.1.1. Palladium-based catalysts on carbonaceous support

Beginning the analysis with the dehydrogenation reaction for H_2 release, early research groups were attracted by carbonaceous substrates produced and/or activated in different ways.

Koh et al. [75] devised the synthesis of novel carbon-supported Pd nanoparticles generated from polyaniline (PANI). The PANI/colloidal silica composites were pyrolyzed at temperatures above 500 °C, then the colloidal silica was removed from the carbonised products with an alkaline solution, and finally Pd nanoparticles were deposited within the mesoporous carbon products (Pd/PDMC). They achieved a turnover frequency (TOF) = 2562 h^{-1} by using a 1 mol L^{-1} concentration of SF, at 80 °C with a catalyst load of 5000 ppm.

Hwang et al. [49] studied a Pd catalyst on a carbon substrate, adjusting both the catalyst loading and salt concentration, and found that a 3 wt% Pd/C loading and a 7 mol L^{-1} formate concentration gave the optimum TOF and hydrogen yield: H_2 yield for all investigated formates turned out to be 92%, whereas the TOF was maximum when AF is used and it was 6190 h^{-1}. As the Table S1 (supplementary materials) shows, raising the salt content increases both the yield and the TOF.

Starting with these first findings, Su et al. [72–87] worked on AF with a Pd load of 5% w/w on activated carbon, by changing the reaction time and salt concentration. A plateau was observed at a reaction time of t = 1.5 h for all concentrations of AF, whilst increasing the AF concentration from 1 mol L^{-1} to 15 mol L^{-1} raises the TOF to 5061 h^{-1}. As a result, 3% Pd/C was found to be the best performing catalyst.

Using palladium as the active phase of the catalyst, Bi et al. [79] devised a new approach including the use of Pd/r-GO. Acting as a single carbon-based matrix, GO sheets are applied for heterogeneous catalysis by anchoring metal nanoparticles on its surface. The research group worked with a 4.8 mol L^{-1} concentration of PF, varying the percentage of metal on the substrate; the best concentration was 1 wt% Pd/r-GO, which gave a hydrogen yield of 96% and a TOF = 11,299 h^{-1}.

Shao et al. [87] conducted both computational and experimental studies demonstrating that co-doping carbon materials with both N and a second heteroatom, such as B, S, or P, can change electronic characteristics and surface polarity, thereby improving catalytic activity. Furthermore, co-doping with two elements with different electronegativity (χ), such as N (χ = 3.04) and P (χ = 2.19), might result in a unique electronic structure with a synergistic coupling effect between heteroatoms. Pd/N,P–C have better efficiency than single-doped carbon materials due to this phenomenon. With a catalyst loading of 5000 ppm at 4.7 wt% Pd/N,P–C, a 4 mol L^{-1} concentration of PF, and an operating temperature of 80 °C, a unitary hydrogen yield could be obtained after 2 h of reaction and a TOF = 3246 h^{-1} was measured after 10 min of reaction.

Fig. 4a shows a comparison of the hydrogen yields of the best performing catalysts. Pd/r-GO and Pd/NP-C are clearly superior catalysts, with Pd/r-GO having the highest TOF. In Fig. 4b, all the catalysts reported in the literature (best reported results) are summarized, compared with the theoretical thermodynamic yield in a closed system (gas volume to liquid volume ratio = 3.0) for a better comparison; the fact that many reported yield are higher than the thermodynamic value is due to the fact that experiments are often carried out in fed-batch or open system, allowing for further conversion.

3.1.2. Palladium-based catalysts on TiO_2

Many studies have been conducted using titanium dioxide, a semiconductor with high reactivity; it can be chemically activated by UV irradiation and used in heterogeneous catalysis with photodeposition techniques [88].

Wang et al. [89] used TiO2-supported Pd nanoparticles of diameters ranging from 2 nm to 14 nm in a 2 mol L^{-1} AF solution and found that those with a size of 2 nm had outstanding activity for formate dehydrogenation, with a TOF value of up to 2184 h^{-1} (after 10 min) at 25 °C.

X. Zhu et al. [90] continued previous studies using TiO2, in particular by working with high-quality crystalline PdO nanoparticles with Kirkendall nanovoids uniformly supported on titanate nanotubes (kv-PdO/TiNTs). At low temperatures, these catalysts have been found to be resistant to formate reforming. At ambient temperature (~ 25 °C), the maximal rate of H_2 production in the dehydrogenation reaction with a 1 mol L^{-1} concentration of SF was in the range of 6.5 mol g^{-1} h^{-1}, yielding a TOF = 2602 h^{-1}. These catalysts have a substantially lower hydrogen output than the others, as seen in Fig. 4a, although the process is carried out at T = 25 °C, which negatively affects both the

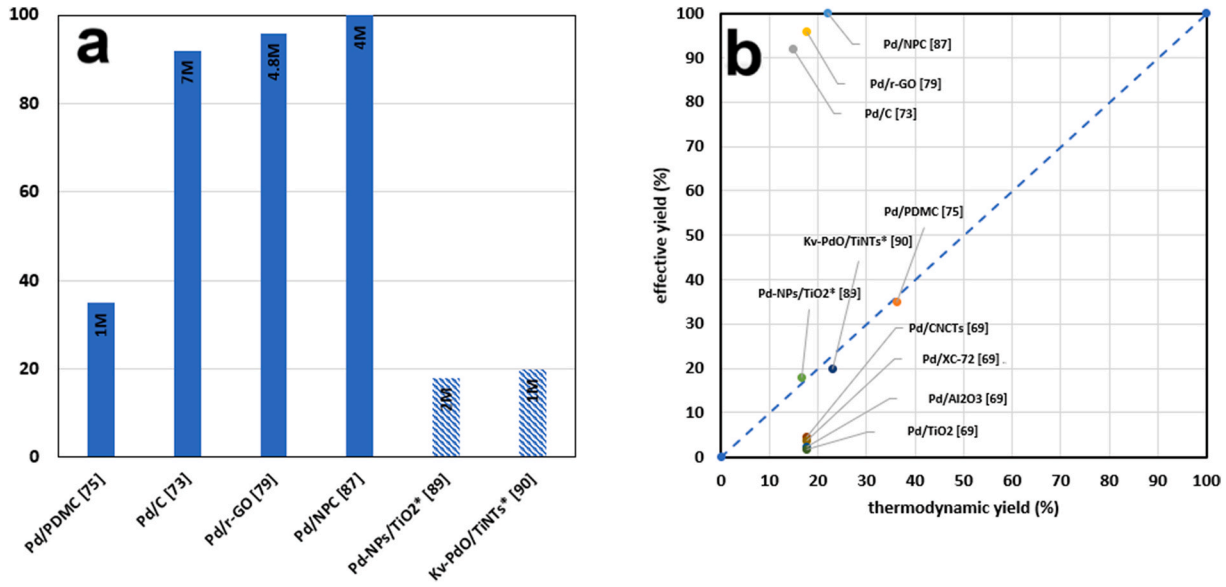

Fig. 4. a) Hydrogen yield (%) at t = 120 min, T = 80 °C (full blue bars) and at t = 90 min, T = 25 °C (dashed bars) for the different reported catalysts; In the columns of the histogram, formate concentrations are indicated for the various catalysts. b) Best performances of all the catalysts proposed in the literature against the thermodynamic conversion value for a closed system.

thermodynamics and the kinetics of the process.

3.1.3. Bimetallic catalysts

Palladium also shows effects when alloyed with other transition metals.

A first step in this direction was taken by S. Masuda et al. [67], who produced a catalyst based on a Pd/Ag alloy that was modified with a TiOx shell supported on TiO_2 (Ag/Pd/TiOx/TiO_2) to improve catalytic activity. The reaction was carried out at 75 °C with a 1 mol L^{-1} concentration of SF and a loading of Pd 1.0 wt% and Ag 0.5 wt%. This material showed significant activity during the dehydrogenation of SF obtaining a TOF = 6499 h^{-1} at 75 °C. The electronic state of Pd had a weaker correlation with the modification of the surface by the application of a TiOx shell on TiO_2-supported Pd–Ag alloy catalysts, indicating that the formation of Pd–TiO_2 interface sites affects activity; in fact, the TOF of the catalyst without the TiOx shell (Ag/Pd/TiO_2) was 5131 h^{-1} under the same adopted conditions.

Other bimetallic catalyst investigations have been carried out by Nakajima et al. [91] developing a catalyst with Pd–Au alloy nanoparticle supported on activated carbon (Pd–Au/AC), which demonstrated better activity than monometallic Pd and Au catalysts. The Au/Pd ratio was varied from 0.1 to 10. The TOF vs. Au/Pd ratio shows a volcano-like relationship in the dehydrogenation reaction, with the catalyst Au–Pd/AC (Ag/Pd molar ratio 1; 4.91 wt % Ag + Pd), having the greatest TOF value.

The reaction was carried out at 1 mol L^{-1} of all the salts of interest, the best being AF, with a hydrogen yield of 5136 mmol g^{-1} h^{-1} and a TOF = 4200 h^{-1}, whereas for SF and PF hydrogen yields were 1848 mmol g^{-1} h^{-1} and 2904 mmol g^{-1} h^{-1}, TOF = 1434 h^{-1} and 1704 h^{-1}, respectively, at T = 40 °C.

The yields of the last two catalysts are shown in Fig. 4a, and it is clear that the values are lower and hence not comparable to those evaluated in the preceding paragraph.

3.2. Hydrogenation reaction

In this paragraph, a thorough analysis for the bicarbonate hydrogenation reaction by heterogeneous catalysts is provided:

$$MHCO_3 + H_2 \rightarrow HCOOM + H_2O \text{ where } M = Na, k, NH_4 \quad (5)$$

For the process to be interesting from an industrial and applicative point of view, it must be cyclable, i.e., the same catalyst should be used to carry out both the hydrogenation and dehydrogenation reactions, which explains why a good number of authors tested their catalyst for both reactions. However, most studies are still preliminary and cyclability will be discussed in Section 3.4.

3.2.1. Palladium-based catalysts on carbonaceous support

Most of the reported Pd-based catalysts use carbonaceous supports. Koh et al. [75] conducted the hydrogenation reaction using the same catalyst (Pd/PDMC) as for dehydrogenation under the same working conditions (5000 ppm and T = 80 °C), in H_2 at 4.0 MPa and obtained a turnover number (TON) = 1625.

Su et al. [72] used a 1 mol L^{-1} solution of the three different salts to investigate the utilization of Pd/AC at 5% wt. Working under the following operating conditions T = 20 °C, P(H_2) = 2.75 MPa, t = 1 h, the best formate yield and the highest TON were obtained using ammonium bicarbonate (NH_4HCO_3, AB) (TON = 782, formate yield = 42.4%), followed by potassium bicarbonate ($KHCO_3$, PB) (TON = 567 formate yield = 30.8%) and sodium bicarbonate ($NaHCO_3$, SB) (TON = 527, formate yield = 28.6%) [69–72]. Starting from AB, different conditions were investigated, changing the reaction time from 1 h to 15 h results in a TON = 1769, formate yield = 95.6%; at t = 2 h and P(H_2) = 5.5 MPa, TON and formate yield were 1672 and 90.4%, respectively, at 20 °C.

Bi et al. [79] used the same catalyst as for dehydrogenation (Pd/r-GO), working with a PB concentration of 4.8 mol L^{-1}, T = 100 °C, P(H_2) = 4.0 MPa, t = 10 h and varying the percentage of active phase on the substrate. They found that 1 wt % Pd/r-GO was the best metal load as for the dehydrogenation reaction.

Working with 1 wt % Pd/r-GO, three different conditions were considered: (i) 6800 ppm of catalyst and a reaction time of t = 32 h; in this case, they obtained the best TON = 7088 and a formate yield 94.5% and (ii) 20,400 ppm of catalyst and reaction time of t = 10 h, obtaining a formate yield of 96.8% and a TON = 2420; finally, increasing the temperature to 130 °C the yield and TON values were 95.6% and 2390 respectively.

Shao et al. [87] conducted the hydrogenation process (Pd/N,P–C) adopting the same double doped support used for dehydrogenation, attaining greater efficiencies than single-doped carbon materials. Working at T = 80 °C, with a P(H_2) = 8.0 MPa, a catalyst loading of

5000 ppm at 4.7 wt% Pd/N,P–C and a 4 mol L^{-1} concentration of PB, the reported formate yields and TON were 94.6% and 4027 for 1.5 h of reaction and 96% and 4269 for 3 h of reaction, respectively.

Wang et al. [92] developed a novel palladium nanoparticle catalyst based on mesoporous carbon doped with nitrogen (Pd/NC) at 4.6 wt% in a 4 mol L^{-1} PB solution. The study tested three different nitriding temperatures: 873, 973, and 1073 K, with 873 K being the best. Using a P(H_2) = 6.0 MPa and altering the reaction duration and temperature: T = 80 °C and t = 2 h resulted in 69.7% formate yield and TON = 1598; T = 60 °C and t = 3 h also resulted in 69.7% formate yield; at T = 40 °C and t = 4 h formate yield was 83.3%. This demonstrate that despite the fact that the reaction yield is favored at low temperatures, kinetic limitations might be severe for some catalysts.

Shao et al. [83] described a Pd nanocatalyst supported on mesoporous graphitic carbon nitride (Pd/mpg-C_3N_4) for reversible hydrogen storage, with promising results in the hydrogenation process.

The Pd/mpg-C_3N_4 catalyst has been demonstrated to work effectively in the hydrogenation of large quantities of bicarbonate under ambient settings. At T = 80 °C, with a catalyst loading of 4000 ppm and a P(H_2) = 6.0 MPa, the different formate yields and TON were investigated using a 1.0 mol L^{-1} concentration of the three different bicarbonates (AB, SB, and PB) with a 2.0 wt% Pd catalyst (2.0 wt% Pd/mpg-C_3N_4) [72]. Contrary to what reported for the effect of the countercation on the reaction yield, different salts can have significant different kinetics, depending on the specific catalyst adopted.

Using PB concentration of 4.0 mol L^{-1} and increasing hydrogen pressure from 2.0 MPa to 8.0 MPa after 3 h of reaction, the formate yield rose from 36% to 71%, while the TON changed from 3252 to 6414. With rising hydrogen pressure, formate yield increases achieving a plateau value, which is consistent with the results of thermodynamic calculations. The increase in temperature from 60 °C to 80 °C is significantly beneficial for the yield and TON, leading to an increases from 28.6% to 43.2% and from 2607 to 5051, respectively.

Also in this case, the performances of the catalysts were compared in Fig. 5a, the best catalysts being Pd/AC, Pd/r-GO, and Pd/N,P–C.

Remarkably, Pd/r-GO has the largest TON value, is extremely efficient for the discharge reaction, and may be the best choice for a cyclic process. In Fig. 5b, all the catalysts reported in the literature (best reported results) are summarized, compared with the theoretical thermodynamic yield in a closed system or a system at constant hydrogen pressure, depending on the case. Contrary to what reported in Fig. 4b for the dehydrogenation step, in this case all reported values are lower than thermodynamic conversion, since the experimental set-ups reflect the calculations. Also in this case, it is clear that Pd/AC, Pd/r-GO, and Pd/N, P–C, are the best reported catalysts since they allow to achieve conversion values very close to their theoretical limit.

3.2.2. *Palladium-based catalysts on TiO_2 and other supports*

Jin et al. [84] conducted an interesting and novel study, in which they investigated the influence of solar radiation adopting a direct technique of hydrogenating bicarbonate to formate on a light-driven Pd/TiO_2 nanocatalyst. Increasing the Pd loading from 4.78 wt % to 8.88 wt %, the yield improves but the TON decreases; therefore, performance were evaluated at the lowest Pd loading. The reaction was carried out at 2.0 mol L^{-1} concentration of PB, under 3.0 MPa of H_2, and a catalyst load of 4000 ppm for 3 h. Formate yield was 13.3% without irradiation, and significantly increased to 59.1% when irradiated with a Xe lamp.

Other substrates that can be activated with the Xe lamp, were tested, such as ZnO, C_3N_4, Al_2O_3, SiO_2 with 5 wt % Pd load.

Working under the same operating conditions (2 mol L^{-1} PB, P(H_2) = 3.0 MPa, cat = 4000 ppm), light irradiation was always beneficial to yield. However, all tested supports performed worse than Pd/TiO_2.

3.2.3. *Bimetallic catalysts*

Masuda et al. [67] designed a Pd/Ag catalyst with a TiOx shell supported on TiO_2 that performs well for the dehydrogenation process. During the hydrogenation, this material showed high activity and a TON of 820. The reaction was carried out at 80 °C with 1 mol L^{-1} SB and a loading of 1.0 wt % Pd and 0.5 wt % Ag.

Zhong et al. [93] used a bimetallic catalyst supported on a phenylenediamine-alkalized reduced graphene oxide (Pd–Au/P-DA-rGO). The hydrogenation reaction of a 0.5 mol L^{-1} solution of PB was carried out under different metal loadings, the optimum being $Pd_{0.50}Au_{0.50}$/PDA-rGO (the Pd/Ag mol/mol ratio is 1). A study was carried out with the goal of optimizing several reaction parameters such as reaction duration, temperature, H_2 pressure, catalyst quantity, and PB concentration.

The PF yield quickly increased to 73% during the first 4 h at 30 °C, finally reaching a maximum of 90% in 16 h, and then stayed constant even after an extension of the reacting period was extended to 24 h, indicating that the reaction had reached equilibrium. At 50 °C and 80 °C,

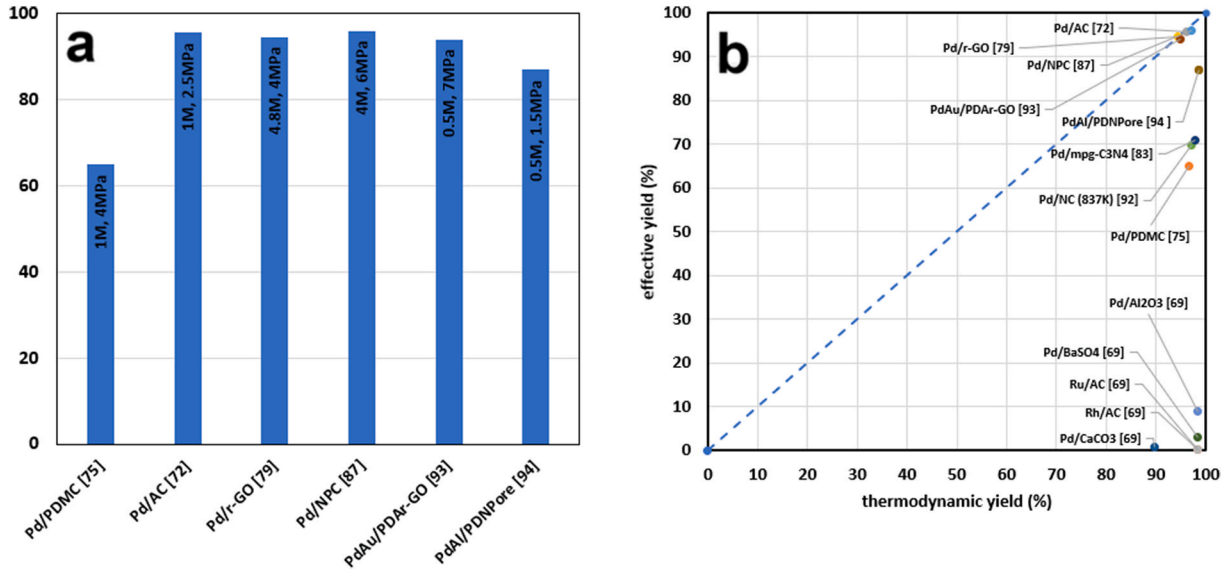

Fig. 5. a) Formate yield (%) at reached plateau. In the columns of the histogram, there are additional information (formate concentrations and H_2 pressure) for the various catalysts. b) best performances of all the catalysts proposed in the literature against the thermodynamic conversion value.

similar results were seen. Although a 91% PF yield was obtained in 6 h at 80 °C, implying a faster reaction rate at higher temperatures, the optimum PF yields at 30 °C, 50 °C, and 80 °C were all very close (90%, 92%, and 91%, respectively), indicating that temperature had little effect on the reaction equilibrium. The negligible influence of temperature on equilibrium yields at the adopted conditions was shown in a recently published thermodynamic analysis [74].

Wang et al. [94] produced a nanoporous catalyst consisting of nanoporous bare Pd with a certain percentage of bare Al (PdAl/PDN-Pore), similarly to what is done to obtain Raney Ni.

The yields varied depending on the Pd/Al ratio; a Pd/Al ratio of 88/12 yields 72% after 24 h using a 0.5 mol L^{-1} SB solution, a catalyst load of 1300 ppm, a H_2 pressure of 1.5 MPa, and T = 80 °C.

The differences between two kinds of alloys are seen in Fig. 5a. The formate yield of the PdAu/PDAr-GO catalyst is 94%, which is comparable to the highest one, i.e. 96 % on Pd/N,P–C.

3.3. Non-active catalysts

A variety of catalysts that do not perform well for this type of reaction have been tested in the literature. In this paragraph, they are summarized for future research direction in the design of new catalytic systems.

Yuan Bi et al. [79] examined several carbonaceous and non-carbonaceous substrates utilizing Pd as catalysts. In the dehydrogenation reaction, two alternative substrates, Al_2O_3 and TiO_2, were utilized; in the hydrogenation reaction, $CaCO_3$ and $BaSO_4$ were also studied, whose yield and TOF were lower by an order of magnitude than those obtained with a carbonaceous support. Su et al. [72] investigated the hydrogenation process using several transition metals (Ru, Rh, Pt, and Ni) on activated carbon support. In every case, no significant conversion was measured. He et al. [95] prepared two Au-based catalysts, one on CeO_2 support and the other on ZrO_2. The dehydrogenation process did not take place under all investigated conditions.

Finally, Wang et al. [94] used non-porous Pd/Al alloy to perform the hydrogenation process. The reaction did not occur demonstrating that a certain level of porosity and exposed surface is crucial to obtain the desired interconversion.

3.4. Cyclability

Catalyst cyclability is an important aspect to investigate since it provides useful insights concerning its durability and consistency, important criteria to consider for industrial applications. Cyclability of a catalyst may be determined in two ways: either by recovering the catalyst and reusing it for the same reaction (half cycle, h-cycle), or by conducting both the dehydrogenation and hydrogenation reactions (complete cycle, c-cycle). This second technique is unquestionably more beneficial in industrial applications since it allows the whole reactive cycle to be completed without the need to recover the catalyst from the solution. Unfortunately, up to date, the adoption of this approach has been scarcely documented in the literature.

Masuda et al. [67] used Ag/Pd/TiO_x/TiO_2 as the catalyst for the dehydrogenation process and obtained a significant reduction in hydrogen production from 100% to 65% after only three h-cycles. Zhu et al. [90] obtained more encouraging findings by adopting kv-PdO-TiNTs as a catalyst, and achieving a practically unaltered hydrogen production after 15 h-cycles. Zhong et al. [93] examined the hydrogenation process and found that $Pd_{0.50}Au_{0.50}$/PDA-rGO catalyst results in a significantly lower formate yield after three h-cycles, with a reduction from 74% to 32%. On the other hand, porous dealloyed Pd/Al alloy (88:12 at.) catalyst achieved an almost unaltered formate yield after ten applications [94]. Adopting Pd/N,P–C, Shao et al. [87] examined the two steps of reaction separately and found that the dehydrogenation reaction provides a nearly unaltered hydrogen production for h-5 cycles, whereas the hydrogenation reaction stays effective for 3 h-cycles.

Pd/PDMC catalyst was used for three consecutive c-cycles, achieving TOF values of 1854 h^{-1}, 1753 h^{-1} and 1477 h^{-1} for the first, second, and third cycles, respectively [75]. Using Pd/AC as the catalyst, Su et al. [72] observed a decrease in the cyclic dehydrogenation/hydrogenation reaction of about 1–2% after 5 c-cycles. Similarly, Bi et al. [79] managed to achieve a yield drop of just 1–2% after 6 cycles using Pd/r-GO catalyst. A summary of the cyclability tests in the literature is given in Table 2.

3.5. Preparation techniques

It is widely recognized that preparation techniques play a crucial role in the morphology of the final catalysts and their performances [96,97]. Among the reviewed catalysts for the catalytic bicarbonate hydrogenation and formate dehydrogenation, efforts have been made in the preparation of supports to increase the exposed catalytic surface and control pores dimensions; metal-deposition techniques influenced nanoparticles dimensions and their electronic state. As for the supports, the most interesting techniques found in the literature consisted in: (i) the oxidative aniline polymerization in the presence of colloidal silica followed by pyrolysis at 800 °C and NaOH treatment to obtain porous carbonaceous supports (BET 1080 m^2 g^{-1}, pores 9.4 nm) [75]; (ii) coprecipitation of a mixture of MgO template and precursors (1, 10-phenanthroline and triphenylphospine followed by thermal treatment at 800 °C under N_2 and acid treatment to remove the MgO template (BET 1420 m^2 g^{-1}, pores 8.0 nm) [87]; (iii) mesoporous carbonaceous materials by hard templating method (BET 995 m^2 g^{-1}) [92]; (iv) unsupported porous Pd/Al alloy obtained by fusion of bare matal ingots followed by NaOH treatment to remove most of Al, as for Raney Ni preparation, residual Al acting as a structural and chemical promoter (BET 39–54 m^2 g^{-1}), as electron transfer from Pd to Al was demonstrated [94]. In the first three presented cases, some of the highest BET values reported in the literature were obtained for this type of catalysts; however, in most cases this did not correspond necessarily to a higher activity or faster kinetics. As for porous dealloyed Pd/Al catalysts, kinetics are not easily deduced, although BET values are in line with the preparation technique. Other supports tested in the literature consist of commercial porous carbon (BET 852 m^2 g^{-1}) [49], graphite oxide [79], activated carbon (BET 1420 m^2 g^{-1}, pores 8 nm) [72], TiO_2 (BET 55 m^2 g^{-1}) [84]. In many cases, commercial binders gave better results that the previously described techniques in terms of kinetics of interconversion.

As for the metal deposition, the most common techniques consists of impregnation of the precursors followed by chemical reduction, Fig. 6a [67,83,84,87,93]. In any case, the result is Pd nanoparticles in the range 1.6–2.4 nm [75,83,87,89]. Interestingly, Shao et al. reported for Pd on activated carbon a ratio between Pd (0) and Pd(II) = 56:44 by XPS analysis [83]. A similar ratio is confirmed by Zhong et al. for bimetallic Pd/Au particles on PDA-rGO catalysts [93].

An interesting exception to impregnation followed by wet chemical

Table 2
Cyclability performance of tested heterogeneous catalysts.

CATALYST	REACTION	NUMBER OF CYCLES	REFERENCE
Ag/Pd/TiO_x/TiO_2	dehydrogenation	3 h-cycles	[67]
kv-PdO-TiNTs	dehydrogenation	15 h-cycles	[90]
Pd/N,P–C	dehydrogenation	5 h-cycles	[87]
Pd/N,P–C	hydrogenation	3 h-cycles	[87]
$Pd_{0.50}Au_{0.50}$/PDA-rGO	hydrogenation	3 h-cycles	[93]
Pd/Al alloy (88:12 at)	hydrogenation	10 h-cycles	[94]
Pd/PDMC	cycle	3 c-cycles	[75]
Pd/AC	cycle	5 c-cycles	[72]
Pd/r-GO catalyst	cycle	6 c-cycles	[79]

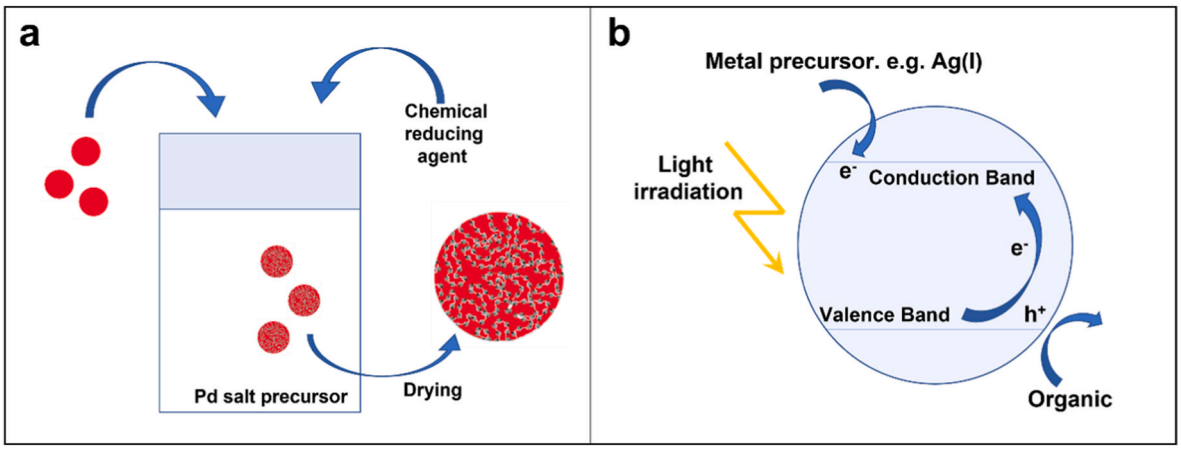

Fig. 6. Main preparation techniques reported in the literature. a) wet impregnation followed by chemical reduction; b) metal photodeposition on semiconductors.

reduction is represented by the catalysts prepared by Masuda et al. [67], Fig. 6b, where this techniques is applied to Pd deposition, but it is followed by the photodeposition of Ag on TiO_2. This represents the only case of photodeposition of metals on semiconductors for the reaction of interest and represents an interesting alternative as photodeposition is generally easier, cheaper, and would allow for the recovery of metals from waste and/or leaching solutions. In this case, XPS analysis confirmed the prevalence of Pd (0). When bimetallic active phases are adopted, usually larger nanoparticles are measured in the range of 3 nm for Pd/Ag [67] or with bimodal distributions (1.8 and 5.0–8.0 nm) for Pd/Au [93]. When the characterization is reported, usually higher Pd loading results in larger nanoparticles [84].

3.6. Effect of countercations and pH

As discussed in Section 2, the effect of the countercation, i.e. NH_4^+, Na^+, and K^+, does not significantly affect the thermodynamics of the transformation and the equilibrium conversion. However, in actual practice it does affect both kinetics of reaction and solubility of the reactant and product.

According to the calculations provided in the literature [74,98], the maximum storage capacity of every system is limited by the solubility of the salts. Formates are always more soluble than bicarbonates; as a result, to avoid precipitation of salts, calculations should be always referred to bicarbonates. Table 3 summarize solubility values of formates and bicarbonates at 20 °C and 80 °C, together with the maximum gravimetric and volumetric hydrogen and energy density. Based on these values, Grubel et al. [73], distinguish between the maximum theoretical storage capacity based on formate solubility and the useable capacity, which is limited by the bicarbonate salt at the reaction temperature. It is worth stressing here, that whilst the energetic density of the solutions increases with temperature, it is significantly limited by bicarbonates solubility.

Based on these considerations potassium and ammonium salts perform much better than sodium [69,73]. However, up to date no experiments have been proposed in the literature using concentration salts higher than their solubility limit. Even though a heterogeneous supersaturated solution might be more difficult to handle from a practical point of view, this would increase storage capacity with no evident shortcomings, since the system is already heterogeneous because of the catalyst presence. Further investigation in this sense are much needed, taking into account the relative interference of formate/bicarbonate on their solubility at different concentrations and temperature.

Different salts have a direct effect on reaction kinetics, depending on the adopted catalyst.

Using Pd/AC [72], Su et al. found that ammonium bicarbonate has a substantially better hydrogenation efficiency than sodium bicarbonate, with the same initial concentration; this is also due to the higher bicarbonate concentration depending on the HCO_3^-/CO_3^{2-} speciation. Precisely, the formate conversion follows the following order: SB < PB < AB under the same experimental conditions.

Therefore, AB produces the highest concentration HCO_3^- in the aqueous solution, leading in the largest hydrogenation reaction formate yield.

Another important aspect is the dehydrogenation of ammonium formate; when the H_2 evolution efficiencies of AF and SF were compared, it was discovered that the H_2 generation rate from SF was significantly slower than that from AF; in fact, comparing both yields after 20 min of reaction shows that the SF yield is only about 70% of AF yield.

Furthermore, K. Nakajima et al. [91] examined the rates of H_2 generation by dehydrogenation of formates (Na and K salts) employing the 1Au1Pd/AC catalyst. The rate of H_2 generation from ammonium formate dehydrogenation was substantially higher than that of K and Na salts.

Shao et al. [83] conducted a further comparison utilizing

Table 3
- Hydrogen energetic density of selected formate and bicarbonate at their solubility limits at 80°C [69,73,99].

	NH_4HCO_2	$NaHCO_2$	$KHCO_2$	NH_4HCO_3	$NaHCO_3$	$KHCO_3$
amount dissolved per 1000 g di H_2O (g) at 80 °C	5330	1380	5800	1090	190	N/A
gravimetric H_2 density at max solubility (gH_2 kg^{-1}) (80 °C)	26.7	17.1	20.3	13.2	3.8	N/A
volumetric H_2 density at max solubility (gH_2 L^{-1}) (80 °C)	32.7	23.6	34.2	16.4	4.2	N/A
gravimetric energy density at max solubility (MJ kg^{-1}) (80 °C)	3.8	2.4	2.9	1.9	0.54	N/A
volumetric energy density at max solubility (MJ L^{-1}) (80 °C)	4.7	3.4	4.9	2.3	0.59	N/A
amount dissolved per 1000 g di H_2O (g) at 20 °C	1430	812	3370	217	96	337
Gravimetric H_2 density at max solubility (gH_2 kg^{-1}) (20 °C)	18.7	13.2	18.3	4.5	2.1	5.0
Volumetric H_2 density at max solubility (gH_2 L^{-1}) (20 °C)	21.2	16.8	29.0	4.8	2.2	5.8
gravimetric energy density at max solubility (MJ kg^{-1}) (20 °C)	2.7	1.9	2.6	0.64	0.30	0.72
volumetric energy density at max solubility (MJ L^{-1}) (20 °C)	3.0	2.4	4.1	0.69	0.31	0.83

Pd/mpg-C_3N_4 as a catalyst. Under the same reaction conditions, PF and SF were used to compare H_2 evolution efficiency. It was discovered that PF had a little greater H_2 evolution efficiency than SF.

In summary, the literature so far shows that ammonium-based systems kinetics are usually faster than in the case of potassium, whereas sodium salts show the worst performances. This is in agreement with the maximum storage capacity for homogeneous aqueous solutions, considering that potassium and ammonium salts are more soluble than sodium salts. Future research on the conversion of supersaturated solutions might overcome the present limitations and further increase volumetric energy density.

Although still scarcely investigated, pH of the solution appears to significantly affect the kinetics of the reaction [18,20,21,26,41]. Most authors taking this variable into account seem to agree that an alkaline solution in the range pH 7.0–9.0 seems to give the best results in terms of both hydrogenation and dehydrogenation reactions. Acidic pH can have strong detrimental effect on the yield of reaction. This could be attributed to speciation of the involved ions and alteration of the surface charge of catalysts, and, as a result, of adsorption equilibria. The formation of bicarbonates during the dehydrogenation reaction tends to increase the pH value of the solution during the reaction. pH has also an influence on bicarbonate/carbonate equilibrium. All the observations suggest that stringent pH control might be required to maximize reaction kinetics, depending on the adopted catalyst.

3.7. Proposed reaction mechanisms

There is no general agreement in the literature on the detailed reaction mechanisms for the investigated catalytic reactions. Moreover, there is no general agreement on the electron transfer between the species and the nature of dissociative hydrogen adsoption (homolytic/heterolytic).

As for Pd catalysts on carbonaceous supports different examples can be found in the literature. For bicarbonate hydrogenation on Pd/mpg-C_3N_4 [83], the suggested mechanism is based on homolytic dissociative H_2 adsorption on Pd and activation of the OH group of bicarbonate on the support, followed by H insertion on carbon and water removal. A similar mechanism is proposed by Jin et al. for Pd over TiO_2 [84], Fig. 7a.

Nakajima et al. [91] and Masuda et al. [67], proposed the activation of bicarbonate by adsoption through the = O group, Fig. 7b. Same activation is hypothesized for formate molecules followed by liquid-phase water insertion for both Pd/Ag on TiO_2 and supported Pd/Au alloy catalyst, Fig. 7d. However the organics are adsorbed on TiO_2 or on Pd/Au particles, respectively. In both cases, H^- insertion is proposed.

Shin et al. [100] used DFT calculations to derive the mechanism on Pd catalyst on N-doped graphite. In this case, bicarbonate is adsorbed on two active sites with the $^-$O groups, whereas H is inserted on the OH group and removed as water, before residual formate desorption, Fig. 7c. For formate dehydrogenation, adsorbed formate dissociates in adsorbed

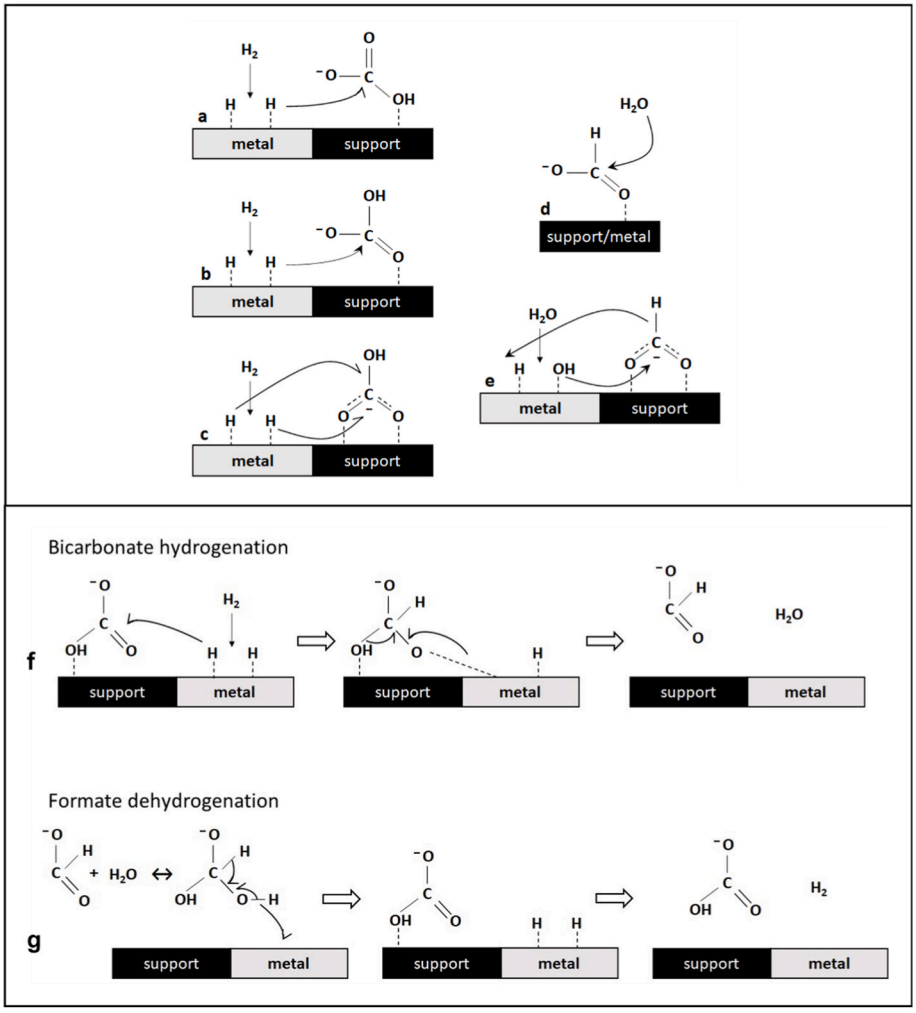

Fig. 7. Main reaction mechanisms proposed in the literature for bicarbonate hydrogenation (a,b,c) and formiate dehydrogenation (d,e); plausible reaction mechanisms for bicarbonate hydrogenation (f) and formate dehydrogenation (g).

CO_2 and H; follows OH^- insertion to form bicarbonate and desorption.

Isotopic experiments for reactions over Pd/PDMC suggested two plausible reaction pathways for the dehydrogenation reaction: molecular formate adsorption and dissociative adsorption of water, follow by OH insertion on C and H_2 desorption is the major pathway, Fig. 7e; minor internal rearrangement of adsorbed formate with CO_2 release is also contemplated [75]. Bicarbonate hydrogenation follows the same mechanism illustrated above for Pd/mpg-C_3N_4 catalysts [83].

Despite the general differences in the mechanisms of organic adsorption/activation, there is a general agreement in the literature on the dissociative H_2 adsorption followed by H insertion for the hydrogenation reaction [92]. Homolytic H_2 dissociation is the most reported mechanism. Based on the conflicting information reported in the literature, plausible reaction mechanisms, based on similarities with the hydrogenation pathways of other organics [101], are proposed in Fig. 7f–g.

3.8. Kinetics and available power

In Section 2, it is reported the assessed potentiality in terms of maximum volumetric density according to the thermodynamic limitations of the system. For practical application, kinetics of hydrogen release is quite important, considering that hydrogen must be fed to a utilizer with a rate that is compatible with the required power. Hydrogenation kinetics is also important to provide feasible recharging time. TON and TOF values reported by the authors are often not directly comparable and cannot provide the necessary information for power calculations. However, in some of the reviewed papers, reaction kinetics data are provided in the form of concentration/yield/released H_2 vs. time. In this Section, these data are manipulated to provide semi-quantitative indications on the maximum power that can be provided by such a system for different scales and applications.

The power generated by hydrogen release P can be calculated according to

$$P = \eta \bullet r \bullet V \bullet \Delta H_c \quad (6)$$

where η is the efficiency of the final utilizer, r is the rate of hydrogen release (mol L^{-1} s^{-1}), V is the volume of the storage vessel (L), and ΔH_c the heat of combustion of hydrogen (285.8 kJ mol^{-1}). In this relation r is considered to be constant with time, which is not the case. However, equation (6) can be used to estimate the order of magnitude of the vessel volume required to provide a certain power to the mechanical system fueled by hydrogen.

From eq. (6), fixing the value of the efficiency, for each chosen power and taking the logarithm of both sides of the equation, a straight line is derived.

The logarithm of the initial reaction rate vs. the logarithm of the storage vessel volume, together with the iso-power curves for different applications and the performances of the catalysts reported in the literature are reported in Fig. 8, using a fixed efficiency of the final utilizer $\eta = 0.50$. The reaction conditions for the data reported in Fig. 8 are summarized in Table 4. The initial reaction rate was calculated from the data provided in the quoted reference from time 0 to the first experimental time. Once again, it must be stated that this does not represent a fair comparison, considering that kinetic data in the papers were not reported for this goal and they are obtained under different operating conditions (Table 4). However, it gives a general idea of the performances that these kinds of catalytic systems may have for real applications. Interestingly, a storage volume vessel in the range of 200 L, which is compatible from a thermodynamic point of view for automotive applications [74], can provide enough power to move cars and trucks, with some of the reported catalytic systems, depending on the specific application. However, if the reaction rate rapidly decreases with time, it may be necessary to increase such volume. As a result, for real application of such systems, research to find stable and fast catalysts is still crucial to reduce time-to-market. Regarding the total amount of hydrogen required for car autonomy, a recently published paper on the formate/bicarbonate system [74] shows that a 180 L solution reservoir would provide up to 857 mol of hydrogen, allowing for 200 km autonomy. This was calculated for homogeneous solutions, but could be further improved if salts are used above their solubility limit. Unfortunately, there is a substantial lack of studies, adopting formate/bicarbonate solutions above their solubility limit as discussed in Section 3.6.

Fewer data are available for hydrogenation kinetics in terms of moles converted per unit time and unit volume, the ones that could be deduced from the literature were summarized in Table 4. As a general trend, hydrogenation kinetics is slower than formate dehydrogenation by one order of magnitude, which suggests that the improvement of catalytic reaction rates for this step may be crucial to reduce the time to recharge the system working with relatively low and safe H_2 pressure. In addition, in case of bicarbonate hydrogenation, reaction rate is not constant with time and initial reaction rate cannot be used for recharge calculations. However, for the sake of comparison the characteristic time of reaction, defined as the ratio between the initial reagent concentration and the initial reaction rate, which quantifies the order of magnitude of the overall reaction time are reported in Table 4.

From the calculated characteristic time, it is clear that the most

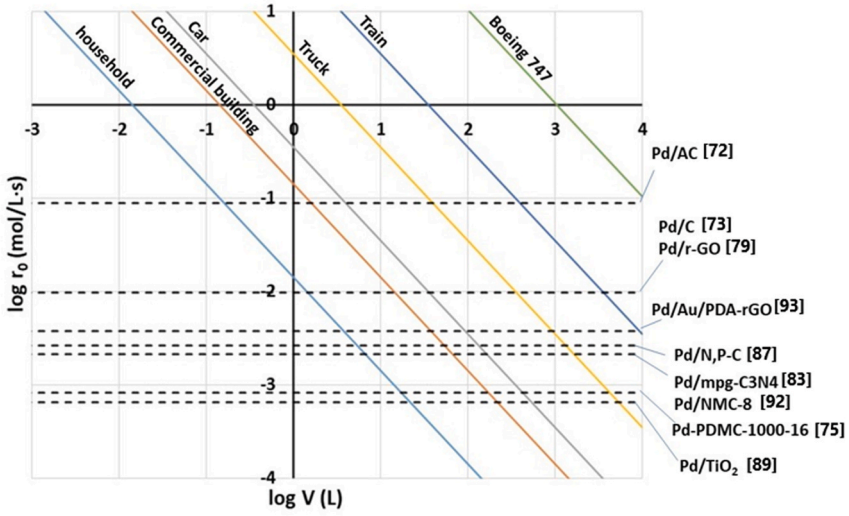

Fig. 8. Initial reaction rate of reported catalysts against required storage volume for specific applications average power. Efficiency of the utilizer = 50%.

Table 4
Calculated initial reaction rate and characteristic time for formates dehydrogenation.

Formate dehydrogenation				
Cat	Ref	r_0 (mol $L^{-1}s^{-1}$)	Conditions	Characteristic time (h)
1 wt % →Pd/r-GO	[79]	$9.75 \cdot 10^{-3}$	4.8 mol L^{-1} HCOOK; Cat: 6811 ppm; T = 90 °C	0.14
1 wt % →Pd-PDMC-1000-16	[75]	$8.20 \cdot 10^{-4}$	1.0 mol L^{-1} HCOONa; Cat: 5000 ppm; T = 80 °C	0.34
3 wt% →Pd/C	[49]	$9.77 \cdot 10^{-3}$	7.0 mol L^{-1} HCOONa; Cat: 30,000 ppm; T = 80 °C	0.2
5 wt% →Pd/AC	[72]	$8.87 \cdot 10^{-2}$	1.0 mol L^{-1} $HCOONH_4$; Cat: 5000 ppm; T = 100 °C	0.0031
4.7 wt% →Pd/N, P–C	[87]	$2.64 \cdot 10^{-3}$	4.0 mol L^{-1} HCOOK; Cat: 5000 ppm; T = 80 °C	0.42
2.0 wt %→ Pd/TiO_2	[89]	$6.48 \cdot 10^{-4}$	2.0 mol L^{-1} $HCOONH_4$; Cat: 500 μmol L^{-1} Pd; T = 60 °C	0.86
5 wt % →kv-PdO/TiNTs	[90]	$1.55 \cdot 10^{-5}$	1.0 mol L^{-1} HCOONa; Cat: 2000 ppm; T = 25 °C	17.88
2.0 wt %→Pd/mpg-C_3N_4	[83]	$2.10 \cdot 10^{-3}$	4.0 mol L^{-1} HCOOK; Cat: 8000 ppm; T = 80 °C	0.53
4.6 wt%→Pd/NMC-8	[92]	$2.12 \cdot 10^{-3}$	2.0 mol L^{-1} HCOOK; Cat: 3333 ppm; T = 60 °C	0.26
Pd w.t% = 9.8, Au wt.% = 17.8 →$Pd_{0.5}Au_{0.5}$/PDA-rGO	[93]	$3.74 \cdot 10^{-3}$	6.0 mol L^{-1} HCOOK; Cat: 15,800 μmol L^{-1} Pd + Au; T = 80 °C	0.45
Bicarbonate hydrogenation				
Cat	**Ref**	**r_0(mol $L^{-1}s^{-1}$)**	**Conditions**	**Characteristic time (h)**
5 wt% →Pd/AC	[72]	$1.15 \cdot 10^{-4}$	1 mol L^{-1} NH_4HCO_3; cat: 5000 ppm; H_2: 2.75 MPa; T = 20 °C	2.41
2.0 wt % <→ Pd/mpg-C_3N_4	[83]	$8.90 \cdot 10^{-4}$	4 mol L^{-1} $KHCO_3$; 4000 ppm cat; H_2: 6.0 MPa; T = 80 °C	1.25
Pd w.t% = 9.8, Au wt.% = 17.8 →$Pd_{0.5}Au_{0.5}$/PDA-rGO	[93]	$6.15 \cdot 10^{-5}$	0.5 mol L^{-1} $KHCO_3$; (Pd + Au)/KHCO3 = $1.83 \cdot 10^{-2}$ H_2: 5.0 MPa; T = 80 °C	2.26
5 wt% →Pd/C	[102]	$1.42 \cdot 10^{-4}$	1 mol L^{-1} $NaHCO_3$; 2000 ppm; H_2: 1 atm (bubbling); T = 25 °C	1.96

suitable catalysts for dehydrogenation kinetics are based on carbonaceous materials at relatively high temperature; considering the ease of preparation, Pd on porous carbon seems to be the most appealing solution to ensure fast kinetics and so high available power. The recharge time is less critical since hydrogen uptake can be operated off-line and take a longer time; however, as expected, high hydrogen pressure and catalyst load decrease the hydrogenation characteristic time; in this case, N-doped carbonaceous materials give the best performances, although palladium on porous carbonaceous materials is operated at lower temperature. Differences between hydrogenation and dehydrogenation kinetics need further investigations and may lead to the utilization of hybrid systems with more catalysts adopted at once.

3.9. Technological implications

Based on the present review, an applicative scenario is pictured in Fig. 9. A heterogeneous storage vessel containing a supersaturated An aqueous rechargeable solution and the catalyst is coupled with a fuel system for power generation for automotive applications. During motion, formate is converted to bicarbonate and hydrogen is generated. During this stage four critical issues to be addressed by future research can be outlined for prototyping: (i) ensure precise operating conditions control kinetics and allow for variable power operations; another option might include an interstage hydrogen vessel to accumulate H_2 during low power operations and discharge it when peak power is required; (ii) finding optimal inter-stage vessels to accumulate and pressurize hydrogen to the pressure required by mobile applications (i.e. up to 5 bars): this may require an additional compressor but it could also be realized by releasing hydrogen in a closed vessel of proper volume, although this might be detrimental for equilibrium conversion; (iii) suspended solid management and mixing; this is always present if supersaturated solutions are used; the solid catalyst can be suspended or immobilized, although this last option requires proper reaction design to avoid mass transfer limitations and might require occasional catalyst replacement; (iv) water evaporation management and occasional inertization of the vessel to enhance conversion.

At the refuelling station exhaust bicarbonate solutions can be discharged and reconverted off-line to fresh formate using pressurized hydrogen. It is worth stressing here that adopting a proper catalytic

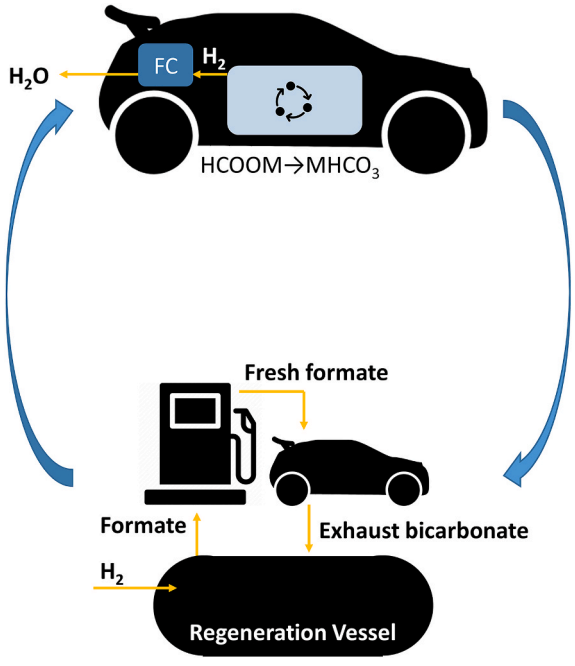

Fig. 9. Example of technological application for the automotive sector.

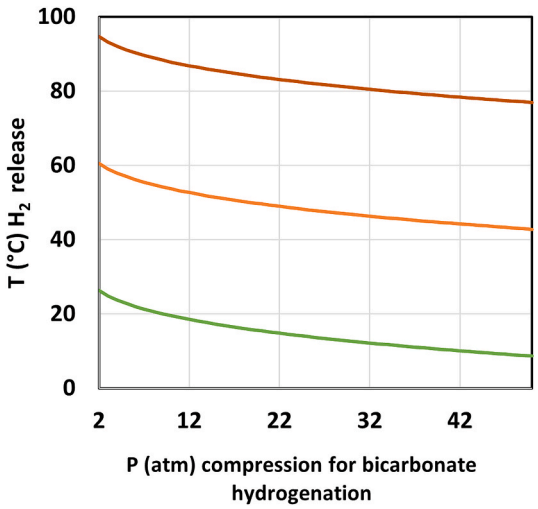

Fig. 10. Energetic efficiency of the formate/bicarbonate system for a 5 mol L^{-1} solution as a function of the dehydrogenation reaction temperature and the hydrogenation reaction pressure.

system, hydrogen pressure can be restrained. The approach would in any case avoid on-board high-pressure H_2 with undeniable advantages from a safety point of view.

To compare the herein reviewed storage system with the well-established H_2 storage technologies, an energetic efficiency calculation was carried out.

For formate/bicarbonate H_2 storage system, energetic efficiency was defined as:

$$\eta = 1 - \frac{Q_h + n_{H_2} \bullet \Delta H_r + W_c}{n_{H_2} \bullet \Delta H_c}$$

Where Q_h is the heat required to bring the aqueous solution to dehydrogenation temperature, n_{H_2} is the number of released H_2 moles, ΔH_r is the dehydrogenation reaction enthalpy, W_c is the compression work to reach the pressure required by the hydrogenation reaction, and ΔH_c the heat released by hydrogen combustion.

The results of the calculations for a 5 mol L^{-1} solution are reported in Fig. 10.

As one can see, efficiency depends on hydrogen release temperature and H_2 pressure required for bicarbonate hydrogenation. In the literature, hydrogen is usually compressed between 20 and 30 bar for bicarbonate hydrogenation, whereas H_2 release reaction is carried out at about 80 °C. In these conditions we obtain an efficiency of about 72%.

This is lower than compressed hydrogen (94%), liquefied hydrogen (77%), and close to lithium batteries (75%). However, it must be stressed that there is room for improvement (up to 90%) if catalytic systems that can work at lower pressure and temperature are found. Also, the heat required to bring the aqueous solution at the required temperature and to sustain the endothermic reaction might be recovered from the heat dissipated by the utilizer, improving the overall process energetic efficiency.

4. Conclusions

Formate/bicarbonate catalytic interconversion is an interesting and promising chemical system for safe and convenient hydrogen uptake and release. Thermodynamic models in different possible configurations show that the system can be efficiently used under proper conditions for a cyclic transformation achieving almost complete conversion. In particular, periodic purge of released hydrogen with an inert gas can allow to achieve complete conversion during formate dehydrogenation, whereas low temperature and modest hydrogen pressure can ensure bicarbonate conversion as high as 98%. Different salts have similar thermodynamics; however; they behave significantly differently in terms of kinetics and solubility, which show that potassium and ammonium salts are more promising than sodium. However, no studies show significant application of supersaturated solutions, which may offer an important alternative to increase energetic density. Preliminary analysis shows that the achievable energetic efficiency ranges from 70 to 90%, depending on the operating conditions for catalytic hydrogenation and dehydrogenation.

In any case, robust catalytic systems that allow for fast kinetics and cyclability are needed. At present, the most promising results have been attained by Pd or Pd alloys supported on porous carbonaceous materials, or less frequently on TiO_2. Most heterogeneous catalysts are synthetized by wet impregnation and chemical reduction, with the only exception of photodeposited metals on semiconductors. Further investigation is needed to investigate coprecipitated catalysts, particularly suited for low temperature reactions, and/or calcined catalysts, as well as other innovative techniques.

For real applications, cyclability of catalysts and kinetics of hydrogen release play a crucial role. However, both aspects are still scarcely investigated in the present literature.

Declaration of competing interest

The authors declare that they have no known competing financial interests or personal relationships that could have appeared to influence the work reported in this paper.

Data availability

No data was used for the research described in the article.

Acknowledgements

This research received no specific grant from any funding body.

Appendix A. Supplementary data

Supplementary data to this article can be found online at https://doi.org/10.1016/j.rser.2022.113102.

References

[1] Yue M, Lambert H, Pahon E, Roche R, Jemei S, Hissel D. Hydrogen energy systems: a critical review of technologies, applications, trends and challenges. Renew Sustain Energy Rev 2021;146:111180. https://doi.org/10.1016/J.RSER.2021.111180.
[2] Demirbas A. Future hydrogen economy and policy. Energy Sources B Energy Econ Plann 2017;12(2):172–81. https://doi.org/10.1080/15567249.2014.950394.
[3] Oliveira AM, Beswick RR, Yan Y. A green hydrogen economy for a renewable energy society. Curr Opin Chem Eng 2021;33:100701. https://doi.org/10.1016/J.COCHE.2021.100701.
[4] Tashie-Lewis BC, Nnabuife SG. Hydrogen production, distribution, storage and power conversion in a hydrogen economy - a technology review. Chem Eng J Adv 2021;8:100172. https://doi.org/10.1016/J.CEJA.2021.100172.
[5] Wang M, Wang G, Sun Z, Zhang Y, Xu D. Review of renewable energy-based hydrogen production processes for sustainable energy innovation. Glob Energy Interconnect 2019;2(5):436–43. https://doi.org/10.1016/J.GLOEI.2019.11.019.
[6] Delpierre M, Quist J, Mertens J, Prieur-Vernat A, Cucurachi S. Assessing the environmental impacts of wind-based hydrogen production in The Netherlands using ex-ante LCA and scenarios analysis. J Clean Prod 2021;299:126866. https://doi.org/10.1016/J.JCLEPRO.2021.126866.
[7] Simpson AP, Lutz AE. Exergy analysis of hydrogen production via steam methane reforming. Int J Hydrogen Energy 2007;32(18):4811–20. https://doi.org/10.1016/j.ijhydene.2007.08.025.
[8] Gao Q, Wang L, Peng W, Zhang P, Chen S. Safety analysis of leakage in a nuclear hydrogen production system. Int J Hydrogen Energy 2022;47(7):4916–31. https://doi.org/10.1016/J.IJHYDENE.2021.11.099.
[9] Pinsky R, Sabharwall P, Hartvigsen J, O'Brien J. Comparative review of hydrogen production technologies for nuclear hybrid energy systems. Prog Nucl Energy 2020;123:103317. https://doi.org/10.1016/J.PNUCENE.2020.103317.

[10] El-Emam RS, Özcan H. Comprehensive review on the techno-economics of sustainable large-scale clean hydrogen production. J Clean Prod 2019;220:593–609. https://doi.org/10.1016/J.JCLEPRO.2019.01.309.
[11] Myslikova Z, Gallagher KS. Mission Innovation is mission critical. Nat Energy 2020;5(10):732–4. https://doi.org/10.1038/s41560-020-00694-5.
[12] The EUROPEAN clean hydrogen alliance reports of the alliance roundtables on barriers and mitigation measures. October 2021; vols. 1–55. https://ec.europa.eu/growth/system/files/2021-11/ECH2A%20RTs%20reports%20on%20barriers%20and%20mitigation%20measures_FINAL.pdf [accessed 15 July 2022].
[13] Park BH, Chae CK. Development of correlation equations on hydrogen properties for hydrogen refueling process by machine learning approach. Int J Hydrogen Energy 2022;47(6):4185–95. https://doi.org/10.1016/J.IJHYDENE.2021.11.053.
[14] Kharel S, Shabani B. Hydrogen as a long-term large-scale energy storage solution to support renewables. Energies 2018;11(10). https://doi.org/10.3390/en11102825.
[15] Mukherjee U, Elsholkami M, Walker S, Fowler M, Elkamel A, Hajimiragha A. Optimal sizing of an electrolytic hydrogen production system using an existing natural gas infrastructure. Int J Hydrogen Energy 2015;40(31):9760–72. https://doi.org/10.1016/J.IJHYDENE.2015.05.102.
[16] Ogden J, Jaffe AM, Scheitrum D, McDonald Z, Miller M. Natural gas as a bridge to hydrogen transportation fuel: insights from the literature. Energy Pol 2017;115:317–29. https://doi.org/10.1016/J.ENPOL.2017.12.049.
[17] Sarkar J, Bhattacharyya S. Application of graphene and graphene-based materials in clean energy-related devices Minghui. Arch Therm 2012;33(4):23–40. https://doi.org/10.1002/er.
[18] Zhou L. Progress and problems in hydrogen storage methods. Renew Sustain Energy Rev 2005;9(4):395–408. https://doi.org/10.1016/J.RSER.2004.05.005.
[19] Thiyagarajan SR, Emadi H, Hussain A, Patange P, Watson M. A comprehensive review of the mechanisms and efficiency of underground hydrogen storage. J Energy Storage 2022;51:104490. https://doi.org/10.1016/J.EST.2022.104490.
[20] Faye O, Szpunar J, Eduok U. A critical review on the current technologies for the generation, storage, and transportation of hydrogen. Int J Hydrogen Energy 2022;47(29):13771–802. https://doi.org/10.1016/J.IJHYDENE.2022.02.112.
[21] Turani-I-Belloto K, Castilla-Martinez CA, Cot D, Petit E, Benarib S, Demirci UB. Nanosized ammonia borane for solid-state hydrogen storage: outcomes, limitations, challenges and opportunities. Int J Hydrogen Energy 2021;46(10):7351–70. https://doi.org/10.1016/J.IJHYDENE.2020.11.224.
[22] Moradi R, Groth KM. Hydrogen storage and delivery: review of the state of the art technologies and risk and reliability analysis. Int J Hydrogen Energy 2019;44(23):12254–69. https://doi.org/10.1016/J.IJHYDENE.2019.03.041.
[23] Zohuri B. Hydrogen energy. Springer International Publishing; 2019.
[24] Heinemann N, Alcade J, Miocic JM, Hangx SJT, Kallmeyer J, Ostertag-Henning C, Hassanpouryouzband A, Thaysen EM, Strobel GJ, Schmidt-Hattenberger C, Edlmann K, Wilkinson M, Bentham M, Haszeldine RS, Carbonell R, Rudloff A. Enabling large-scale hydrogen storage in porous media-the scientific challenges. Energy Environ Sci 2021;14(2):853–64. https://doi.org/10.1039/d0ee03536j.
[25] Yang F, Wang J, Zhang Y, Wu Z, Zhang Z, Zhao F, Huot J, Navakovic JG, Novakovic N. Recent progress on the development of high entropy alloys (HEAs) for solid hydrogen storage: a review. Int J Hydrogen Energy 2022;47(21):11236–49. https://doi.org/10.1016/J.IJHYDENE.2022.01.141.
[26] Chanchetti LF, Leiva DR, Lopes de Faria LI, Ishikawa TT. A scientometric review of research in hydrogen storage materials. Int J Hydrogen Energy 2020;45(8):5356–66. https://doi.org/10.1016/J.IJHYDENE.2019.06.093.
[27] Jain IP, Jain P, Jain A. Novel hydrogen storage materials: a review of lightweight complex hydrides. J Alloys Compd 2010;503(2):303–39. https://doi.org/10.1016/J.JALLCOM.2010.04.250.
[28] Wei TY, Lim KL, Tseng YS, Chan SLI. A review on the characterization of hydrogen in hydrogen storage materials. Renew Sustain Energy Rev 2017;79:1122–33. https://doi.org/10.1016/J.RSER.2017.05.132.
[29] Niaz S, Manzoor T, Pandith AH. Hydrogen storage: materials, methods and perspectives. Renew Sustain Energy Rev 2015;50:457–69. https://doi.org/10.1016/J.RSER.2015.05.011.
[30] Rivard E E, Trudeau M, Zaghib K. Hydrogen storage for mobility: a review. Materials 2019;12(12):1973. https://doi.org/10.3390/ma12121973.
[31] Ramirez-Vidal P, Canavesi RLS, Sdanghi G, Schaefer S, Maranzana G, Celzard A, Fierro V. A step forward in understanding the hydrogen adsorption and compression on activated carbons. ACS Appl Mater Interfaces 2021;13(10):12562–74. https://doi.org/10.1021/acsami.0c22192.
[32] Zivar D, Kumar S, Foroozesh J. Underground hydrogen storage: a comprehensive review. Int J Hydrogen Energy 2021;46(45):23436–62. https://doi.org/10.1016/j.ijhydene.2020.08.138.
[33] Tarhan C, Çil MA. A study on hydrogen, the clean energy of the future: hydrogen storage methods. J Energy Storage 2021;40:102676. https://doi.org/10.1016/j.est.2021.102676.
[34] Mohan M, Sharma VK, Kumar EA, Gayathri V. Hydrogen storage in carbon materials-A review. Energy Storage 2019. https://doi.org/10.1002/est2.35.
[35] Durbin DJ, Malardier-Jugroot C. Review of hydrogen storage techniques for on board vehicle applications. Int J Hydrogen Energy 2013;38(34):14595–617. https://doi.org/10.1016/j.ijhydene.2013.07.058.
[36] Sdanghi G, Maranzana G, Celzard A, Fierro V. Review of the current technologies and performances of hydrogen compression for stationary and automotive applications. Renew Sustain Energy Rev 2019;102:150–70. https://doi.org/10.1016/j.rser.2018.11.028.
[37] Langmi HW, Ren J, North B, Mathe M, Bessarabov D. Hydrogen storage in metal-organic frameworks: a review. Electrochim Acta 2014;128:368–92. https://doi.org/10.1016/j.electacta.2013.10.190.
[38] Ren J, Musyoka NM, Langmi HW, Mathe M, Liao S. Current research trends and perspectives on materials-based hydrogen storage solutions: a critical review. Int J Hydrogen Energy 2017;42(1):289–311. https://doi.org/10.1016/j.ijhydene.2016.11.195.
[39] Hassan IA, Ramadan HS, Saleh MA, Hissel D. Hydrogen storage technologies for stationary and mobile applications: review, analysis and perspectives. Renew Sustain Energy Rev 2021;149:111311. https://doi.org/10.1016/j.rser.2021.111311.
[40] Moradi R, Groth KM. Hydrogen storage and delivery: review of the state of the art technologies and risk and reliability analysis. Int J Hydrogen Energy 2019;44(23):12254–69. https://doi.org/10.1016/j.ijhydene.2019.03.041.
[41] Ouyang L, Liu F, Wang H, Liu J, Yang XS, Sun L, Zhu A. Magnesium-based hydrogen storage compounds: a review. J Alloys Compd 2020;832:154865. https://doi.org/10.1016/j.jallcom.2020.154865.
[42] Aziz M, TriWijayanta A, Nandiyanto ABD. Ammonia as effective hydrogen storage: a review on production, storage and utilization. Energies 2020;13(12):1–25. https://doi.org/10.3390/en13123062.
[43] Underground R Tarkowski R. Hydrogen storage: characteristics and prospects. Renew Sustain Energy Rev 2019;105:86–94. https://doi.org/10.1016/j.rser.2019.01.051.
[44] Yadav M, Xu Q. Liquid-phase chemical hydrogen storage materials. Energy Environ Sci 2012;5(12):9698–725. https://doi.org/10.1039/c2ee22937d.
[45] Wang L, Yang RT. Hydrogen storage on carbon-based adsorbents and storage at ambient temperature by hydrogen spillover. Catal Rev - Sci Eng 2010;52(4):411–61. https://doi.org/10.1080/01614940.2010.520265.
[46] Dagdougui H, Sacile R, Bersani C, Ouammi A. Hydrogen storage and distribution: implementation scenarios. Hydrog Infrastruct Energy Appl 2018:37–52. https://doi.org/10.1016/b978-0-12-812036-1.00004-4.
[47] Purewal J, Veenstra M, Tamburello D, Ahmed A, Matzger AJ, Wong-Foy AG, Seth S, Liu Y, Siegel DJ. Estimation of system-level hydrogen storage for metal-organic frameworks with high volumetric storage density. Int J Hydrogen Energy 2019;44(29):15135–45. https://doi.org/10.1016/j.ijhydene.2019.04.082.
[48] Sule R, Mishra AK, Nkambule TT. Recent advancement in consolidation of MOFs as absorbents for hydrogen storage. Int J Energy Res 2021;45(9):12481–99. https://doi.org/10.1002/er.6608.
[49] Li HW, Yan Y, Orimo SI, Züttel A, Jensen CM. Recent progress in metal borohydrides for hydrogen storage. Energies 2011;4(1):185–214. https://doi.org/10.3390/en4010185.
[50] Zhao L, Xu F, Zhang C, Wang Z, Ju H, Gao X, Zhang X, Sun L, Liu Z. Enhanced hydrogen storage of alanates: recent progress and future perspectives. Prog Nat Sci Mater Int 2021;31(2):165–79. https://doi.org/10.1016/J.PNSC.2021.01.007.
[51] Milanese C, Garroni S, Gennari F, Marini A, Klassen T, Dornheim M, Pistidda C. Solid state hydrogen storage in alanates and alanate-based compounds: a review. Metals 2018;8(8):1–15. https://doi.org/10.3390/met8080567.
[52] Demirci UB. Ammonia borane, a material with exceptional properties for chemical hydrogen storage. Int J Hydrogen Energy 2017;42(15):9978–10013. https://doi.org/10.1016/J.IJHYDENE.2017.01.154.
[53] Qiu S, Chu H, Zou Y, Xiang C, Xu F, Sun L. Light metal borohydrides/amides combined hydrogen storage systems: composition, structure and properties. J Mater Chem 2017;5(48):25112–30. https://doi.org/10.1039/c7ta09113c.
[54] Wang K, Pan Z, Yu X. Metal B-N-H hydrogen-storage compound: development and perspectives. J Alloys Compd 2019;794:303–24. https://doi.org/10.1016/J.JALLCOM.2019.04.240.
[55] Huang Y, Cheng Y, Zhang J. A review of high density solid hydrogen storage materials by pyrolysis for promising mobile applications. Ind Eng Chem Res 2021;60(7):2737–71. https://doi.org/10.1021/acs.iecr.0c04387.
[56] Modisha PM, Ouma CNM, Garidzirai R, Wasserscheid P, Bessarabov D. The prospect of hydrogen storage using liquid organic hydrogen carriers. Energy Fuel 2019;33(4):2778–96. https://doi.org/10.1021/acs.energyfuels.9b00296.
[57] He T, Pei Q, Chen P. Liquid organic hydrogen carriers. J Energy Chem 2015;24(5):587–94. https://doi.org/10.1016/j.jechem.2015.08.007.
[58] Byun M, Lee A, Cheon S, Kim H, Lim H. Preliminary feasibility study for hydrogen storage using several promising liquid organic hydrogen carriers: technical, economic, and environmental perspectives. Energy Convers Manag 2022;268:116001. https://doi.org/10.1016/j.enconman.2022.116001.
[59] Zhong H, Ouyang LZ, Ye JS, Liu JW, Wang H, Yao XD, Zhu M. An one-step approach towards hydrogen production and storage through regeneration of NaBH4. Energy Storage Mater 2017;7:222–8. https://doi.org/10.1016/j.ensm.2017.03.001.
[60] Graetz J. Metastable metal hydrides for hydrogen storage. ISRN Mater Sci 2012:1–18. https://doi.org/10.5402/2012/863025.
[61] von Colbe JB, Ares JR, Barale J, Barrico M, Buckley C, Capurso G, Gallandat N, Grant DM, Guzik MN, Jacob I, Jensen EH, Jensen T, Jepsen J, Klassen T, Lototskyy MV, Manickam K, Montone A, Puszkiel J, Dornheim M. Application of hydrides in hydrogen storage and compression: achievements, outlook and perspectives. Int J Hydrogen Energy 2019;44(15):7780–808. https://doi.org/10.1016/j.ijhydene.2019.01.104.
[62] Ley MB, Meggouh M, Moury R, Peinecke K, Felderhoff M. Development of hydrogen storage tank systems based on complex metal hydrides. Materials 2015;8(9):5891–921. https://doi.org/10.3390/ma8095280.
[63] Ruslan N, Yahya MS, Sissique MNI, Yengantiwar AP, Ismail M, Awal MR, Yusoff MZM, Yap MFAAH, Mustafa NS. Review on magnesium hydride and

sodium borohydride hydrolysis for hydrogen production. Crystals 2022;12(10): 1376. https://doi.org/10.3390/cryst12101376.
[64] Lang C, Jia Y, Yao X. Recent advances in liquid-phase chemical hydrogen storage. Energy Storage Mater 2020;26:290–312. https://doi.org/10.1016/J.ENSM.2020.01.010.
[65] Luo Q, Beller M, Jiao H. Formic acid dehydrogenation on surfaces - a review of computational aspect. J Theor Comput Chem 2013;12(7):1330001. https://doi.org/10.1142/S0219633613300012.
[66] Müller K, Brooks K, Autrey T. Hydrogen storage in formic acid: a comparison of process options. Energy Fuel 2017;31(11):12603–11. https://doi.org/10.1021/acs.energyfuels.7b02997.
[67] Masuda S, Shimoji Y, Mori K, Kuwahara Y, Yamashita H. Interconversion of formate/bicarbonate for hydrogen storage/release: improved activity following sacrificial surface modification of a Ag@Pd/TiO2Catalyst with a TiO xShell. ACS Appl Energy Mater 2020;3(6):5819–29. https://doi.org/10.1021/acsaem.0c00744.
[68] Fellay C, Dyson PJ, Laurenczy G. A viable hydrogen-storage system based on selective formic acid decomposition with a ruthenium catalyst. Angew Chem Int Ed 2008;47(21):3966–8. https://doi.org/10.1002/anie.200800320.
[69] Bahuguna A, Sasson Y. Formate-bicarbonate cycle as a vehicle for hydrogen and energy storage. ChemSusChem 2021;14(5):1258–83. https://doi.org/10.1002/cssc.202002433.
[70] Li Z, Pan X, Meng X, Ma J. Study on the harm effects of releases from liquid hydrogen tank by consequence modeling. Int J Hydrogen Energy 2012;37(22): 17624–9. https://doi.org/10.1016/J.IJHYDENE.2012.05.141.
[71] Eppinger J, Huang KW. Formic acid as a hydrogen energy carrier. ACS Energy Lett 2017;2(1):188–95. https://doi.org/10.1021/acsenergylett.6b00574.
[72] Su J, Yang L, Lu M, Lin H. Highly efficient hydrogen storage system based on ammonium bicarbonate/formate redox equilibrium over palladium nanocatalysts. ChemSusChem 2015;8(5):813–6. https://doi.org/10.1002/cssc.201403251.
[73] Grubel K, Su J, Kothandaraman J, Brooks K, Somorjai GA, Autrey T. Research requirements to move the bar forward using aqueous formate salts as H2 carriers for energy storage applications. J Energy Power Technol 2020;2(4). https://doi.org/10.21926/jept.2004016.
[74] Russo D, Calabrese M, Marotta R, Andreozzi R, Di Benedetto A. Thermodynamics of the cyclic formate/bicarbonate interconversion for hydrogen storage. Int J Hydrogen Energy 2022;47(73):31370–80. https://doi.org/10.1016/j.ijhydene.2022.07.033.
[75] Koh K, Jeon M, Chevrier DM, Zhang P, Yoon CW, Asefa T. Novel nanoporous N-doped carbon-supported ultrasmall Pd nanoparticles: efficient catalysts for hydrogen storage and release. Appl Catal B Environ 2017;203:820–8. https://doi.org/10.1016/j.apcatb.2016.10.080.
[76] Guo XT, Zhang J, Chi JC, Li ZH, Liu YC, Liu XR, Zhang SY. Efficient dehydrogenation of a formic acid-ammonium formate mixture over Au3Pd1catalyst. RSC Adv 2019;9(11):5995–6002. https://doi.org/10.1039/c8ra09534e.
[77] Lu M, Zhang J, Yao Y, Sun J, Wang Y, Lin H. Renewable energy storage via efficient reversible hydrogenation of piperidine captured CO2. Green Chem 2018; 20:4292–8. https://doi.org/10.1039/C8GC00954F.
[78] Hwang YJ, Kwon Y, Kim Y, Sohn H, Nam SW, Kim J, Autrey T, Yoon CW, Jo YS, Jeong H. Development of an autothermal formate-based hydrogen generator: from optimization of formate dehydrogenation conditions to thermal integration with fuel cells. ACS Sustainable Chem Eng 2020;8(26):9846–56. https://doi.org/10.1021/acssuschemeng.0c02775.
[79] Bi QY, Lin JD, Liu YM, Du XL, Wang JQ, He HY, Cao Y. An aqueous rechargeable formate-based hydrogen battery driven by heterogeneous Pd catalysis. Angew Chem Int Ed 2014;53(49):13583–7. https://doi.org/10.1002/anie.201409500.
[80] Liu Q, Wu L, Gülak S, Rockstroh N, Jackstell R, Beller M. Towards a sustainable synthesis of formate salts: combined catalytic methanol dehydrogenation and bicarbonate hydrogenation. Angew Chem Int Ed 2014;53(27):7085–8. https://doi.org/10.1002/anie.201400456.
[81] Luo Q, Wang T, Beller M, Jiao H. Hydrogen generation from formic acid decomposition on Ni(2 1 1), Pd(2 1 1) and Pt(2 1 1). J Mol Catal 2013;379: 169–77. https://doi.org/10.1016/j.molcata.2013.08.015.
[82] Bulushev DA, Zacharska M, Beloshapkin S, Guo Y, Yuranov I. Catalytic properties of PdZn/ZnO in formic acid decomposition for hydrogen production. Appl Catal Gen 2018;561:96–103. https://doi.org/10.1016/j.apcata.2018.05.025.
[83] Shao X, Xu J, Huang Y, Su X, Duan H, Wang X. Pd@C3N4 nanocatalyst for highly efficient hydrogen storage system based on potassium bicarbonate/formate. AIChE J 2016;62(7):2410–8. https://doi.org/10.1002/aic.15218.
[84] Jin B, Ye X, Zhong H, Jin F. Light-driven hydrogenation of bicarbonate into formate over nano-Pd/TiO2. ACS Sustain.Chem Eng 2020;8(17):6798–805. https://doi.org/10.1021/acssuschemeng.0c01616.
[85] Alberico E, Leischner T, Junge H, Kammer A, Sang R, Seifert J, Baumann W, Spannenberg A, Junge K, Beller M. HCOOH disproportionation to MeOH promoted by molybdenum PNP complexes. Chem Sci 2021;12(39):13101–19. https://doi.org/10.1039/d1sc04181a.
[86] Hwang YJ, Kwon Y, Kim Y, Sohn H, Nam SW, Kim J, Autrey T, Yoon CW, Jo YS, Jeong H. Development of an autothermal formate-based hydrogen generator: from optimization of formate dehydrogenation conditions to thermal integration with fuel cells. ACS Sustain.Chem Eng 2020;8(26):9846–56. https://doi.org/10.1021/acssuschemeng.0c02775.
[87] Shao X, Miao X, Zhang T, Wang W, Wang J, Ji X. Pd nanoparticles supported on N- and P-Co-doped carbon as catalysts for reversible formate-based chemical hydrogen storage. ACS Appl Nano Mater 2020;3(9):9209–17. https://doi.org/10.1021/acsanm.0c01830.
[88] Etacheri V, Di Valentin C, Schneider J, Bahnemann D, Pillai SC. Visible-light activation of TiO2 photocatalysts: advances in theory and experiments. J Photochem Photobiol C Photochem Rev 2015;25:1–29. https://doi.org/10.1016/J.JPHOTOCHEMREV.2015.08.003.
[89] Wang J, Tan H, Jiang D, Zhou K. Enhancing H2 evolution by optimizing H adatom combination and desorption over Pd nanocatalyst. Nano Energy 2017;33: 410–7. https://doi.org/10.1016/j.nanoen.2017.02.001.
[90] Zhu X, Du L, Guo S, Chen S, Wu B, Liu X, Yan X, Takeuchi N, Kobayashi H, Li R. Tandem catalysis induced by hollow PdO: highly efficient H2 generation coupled with organic dye degradation: via sodium formate reforming. Catal Sci Technol 2018;8(23):6217–27. https://doi.org/10.1039/c8cy01551a.
[91] Nakajima K, Tominaga M, Waseda M, Miura H, Shishido T. Highly efficient supported palladium-gold alloy catalysts for hydrogen storage based on ammonium bicarbonate/formate redox cycle. ACS Sustainable Chem Eng 2019;7 (7):6522–30. https://doi.org/10.1021/acssuschemeng.8b04698.
[92] Wang F, Xu J, Shao X, Su X, Huang Y, Zhang T. Palladium on nitrogen-doped mesoporous carbon: a bifunctional catalyst for formate-based, carbon-neutral hydrogen storage. ChemSusChem 2016;9(3):246–51. https://doi.org/10.1002/cssc.201501376.
[93] Zhong H, Iguchi M, Chatterjee M, Ishizaka T, Kitta M, Xu Q, Kawanami H. Interconversion between CO2 and HCOOH under basic conditions catalyzed by PdAu nanoparticles supported by amine-functionalized reduced graphene oxide as a dual catalyst. ACS Catal 2018;8(6):5355–62. https://doi.org/10.1021/acscatal.8b00294.
[94] Wang J, Zhou CC, Gao Z, Feng X, Yamamoto Y, Bao M. Unsupported nanoporous palladium catalyst for highly selective hydrogenation of carbon dioxide and sodium bicarbonate into formate. ChemCatChem 2021;13(11):2702–8. https://doi.org/10.1002/cctc.202100148.
[95] He L, Ni J, Wang LC, Yu FJ, Cao Y, He HY, Fan KN. Aqueous room-temperature gold-catalyzed chemoselective transfer hydrogenation of aldehydes. Chem Eur J 2009;15(44):11833–6. https://doi.org/10.1002/chem.200901261.
[96] Védrine JC. Concluding remarks and challenges of heterogeneous catalysis on metal oxides. Met Oxides Heterog Catal 2018:551–69. https://doi.org/10.1016/B978-0-12-811631-9.00009-0.
[97] Védrine JC. Importance, features and uses of metal oxide catalysts in heterogeneous catalysis. Chin J Catal 2019;40(11):1627–36. https://doi.org/10.1016/S1872-2067(18)63162-6.
[98] Grubel K, Jeong H, Yoon CW, Autrey T. Challenges and opportunities for using formate to store, transport, and use hydrogen. J Energy Chem 2020;41:216–24. https://doi.org/10.1016/J.JECHEM.2019.05.016.
[99] Dean John A, Lange. Lange's handbook of chemistry. New York: McGraw-Hill; 1999. https://doi.org/10.1080/10426919008953291.
[100] Shin DY, Kim MS, Kwon JA, Shin YJ, Yoon CW, Lim DH. Fundamental mechanisms of reversible dehydrogenation of formate on N-doped graphene-supported Pd nanoparticles. J Phys Chem C 2019;123(3):1539–49. https://doi.org/10.1021/acs.jpcc.8b07002.
[101] Rylander PN. Catalytic hydrogenation in organic synthesis. Elsevier; 1979.
[102] González E, Marchant C, Sepulveda C, Garcia R, Ghampson IT, Escalona N, Garcia-Ferro JL. Hydrogenation of sodium hydrogen carbonate in aqueous phase using metal/activated carbon catalysts. Appl Catal B Environ 2018;224:368–75. https://doi.org/10.1016/j.apcatb.2017.10.038.